A&A 567, A5 (2014)
DOI: 10.1051/0004-6361/201322944

Astronomy & Astrophysics

The *Gaia*-ESO Survey: the Galactic thick to thin disc transition⋆,⋆⋆

A. Recio-Blanco[1], P. de Laverny[1], G. Kordopatis[2], A. Helmi[3], V. Hill[1], G. Gilmore[2], R. Wyse[4], V. Adibekyan[5], S. Randich[6], M. Asplund[7], S. Feltzing[8], R. Jeffries[9], G. Micela[10], A. Vallenari[11], E. Alfaro[12], C. Allende Prieto[13], T. Bensby[8], A. Bragaglia[14], E. Flaccomio[10], S. E. Koposov[2,20], A. Korn[15], A. Lanzafame[16], E. Pancino[14,17], R. Smiljanic[18,19], R. Jackson[9], J. Lewis[2], L. Magrini[6], L. Morbidelli[6], L. Prisinzano[10], G. Sacco[6], C. C. Worley[2], A. Hourihane[2], M. Bergemann[2], M. T. Costado[12], U. Heiter[15], P. Joffre[2], C. Lardo[14], K. Lind[2], and E. Maiorca[6]

(Affiliations can be found after the references)

Received 29 October 2013 / Accepted 28 March 2014

ABSTRACT

Aims. The nature of the thick disc and its relation to the thin disc is presently an important subject of debate. In fact, the structural and chemo-dynamical transition between disc populations can be used as a test of the proposed models of Galactic disc formation and evolution.
Methods. We used the atmospheric parameters, [α/Fe] abundances, and radial velocities, which were determined from the *Gaia*-ESO Survey GIRAFFE spectra of FGK-type stars (first nine months of observations) to provide a chemo-kinematical characterisation of the disc stellar populations. We focussed on a subsample of 1016 stars with high-quality parameters, covering the volume $|Z| < 4.5$ kpc and R in the range 2–13 kpc.
Results. We have identified a thin to thick disc separation in the [α/Fe] vs. [M/H] plane, thanks to the presence of a low-density region in the number density distribution. The thick disc stars seem to lie in progressively thinner layers above the Galactic plane, as metallicity increases and [α/Fe] decreases. In contrast, the thin disc population presents a constant value of the mean distance to the Galactic plane at all metallicities. In addition, our data confirm the already known correlations between V_ϕ and [M/H] for the two discs. For the thick disc sequence, a study of the possible contamination by thin disc stars suggests a gradient up to 64 ± 9 km s^{-1} dex^{-1}. The distributions of azimuthal velocity, vertical velocity, and orbital parameters are also analysed for the chemically separated samples. Concerning the gradients with galactocentric radius, we find, for the thin disc, a flat behaviour of the azimuthal velocity, a metallicity gradient equal to -0.058 ± 0.008 dex kpc^{-1} and a very small positive [α/Fe] gradient. For the thick disc, flat gradients in [M/H] and [α/Fe] are derived.
Conclusions. Our chemo-kinematical analysis suggests a picture where the thick disc seems to have experienced a settling process, during which its rotation increased progressively and, possibly, the azimuthal velocity dispersion decreased. At [M/H] ≈ -0.25 dex and [α/Fe] ≈ 0.1 dex, the mean characteristics of the thick disc in vertical distance to the Galactic plane, rotation, rotational dispersion, and stellar orbits' eccentricity agree with that of the thin disc stars of the same metallicity, suggesting a possible connection between these two populations at a certain epoch of the disc evolution. Finally, the results presented here, based only on the first months of the *Gaia* ESO Survey observations, confirm how crucial large high-resolution spectroscopic surveys outside the solar neighbourhood are today for our understanding of the Milky Way history.

Key words. Galaxy: abundances – Galaxy: disk – Galaxy: stellar content – stars: abundances

1. Introduction

Understanding the chemo-dynamical evolution of the Milky Way disc stellar populations is a crucial step toward reconstructing the history of our Galaxy. This approach can shed new light on the detailed processes that led the Milky Way to form and evolve as a disc-type galaxy, in the more general context of galaxy evolution. In particular, since the first works highlighting the existence of the Milky Way's thin/thick disc dichotomy (Yoshii 1982; Gilmore & Reid 1983), the study of the structural and chemo-dynamical transition between the two disc populations has opened new pathways to constrain Galactic evolution models. Supported by the hierarchical formation of galaxies in the ΛCDM paradigm, external mechanisms have been invoked to explain the chemo-dynamical characteristics of thick disc stars. Among them, the accretion of dwarf galaxies (e.g. Statler 1988; Abadi et al. 2003) and minor mergers of satellites (e.g. Quinn et al. 1993; Villalobos & Helmi 2008) heating the disc dynamically, have been proposed. Similarly, Jones & Wyse (1983) and Brook et al. (2004, 2007) have proposed that the thick disc would have been formed from the collapse produced by the accretion of a gas-rich merger. On the other hand, purely internal formation mechanisms have also been proposed, such as the early turbulent phase of the primordial disc (e.g. Bournaud et al. 2009) and the stars' radial migration due to resonances with the spiral structure or the bar of the Milky Way (e.g. Schönrich & Binney 2009c; Minchev & Famaey 2010; Loebman et al. 2011), although see also Minchev et al. (2012). The relative importance of the different proposed physical processes of evolution can now be tested with increasing robustness thanks to the Galactic spectroscopic surveys targeting the disc stars.

Spectroscopic studies of the disc populations were initially based on kinematically selected samples of solar neighbourhood stars (e.g. Prochaska et al. 2000; Fuhrmann 2004; Bensby et al. 2005; Reddy et al. 2006), with some exceptions such as Edvardsson et al. (1993) or Fuhrmann (1998). In the classical picture that emerged from those studies, the thick disc population is characterized as kinematically hotter than the thin

⋆ Based on observations collected with the FLAMES spectrograph at the VLT/UT2 telescope (Paranal Observatory, ESO, Chile), for the *Gaia*-ESO Large Public Survey, programme 188.B-3002.
⋆⋆ Full Table 1 is only available at the CDS via anonymous ftp to cdsarc.u-strasbg.fr (130.79.128.5) or via http://cdsarc.u-strasbg.fr/viz-bin/qcat?J/A+A/567/A5

disc one (Casetti-Dinescu et al. 2011) and, therefore, composed of stars moving in Galactic orbits with a higher scale height (~900 pc vs. ~300 pc, e.g. Jurić et al. 2008). In addition, the thick disc metallicity distribution peaks at lower values (~−0.5 dex compared to ~–0.2 dex for the thin disc, e.g. Wyse & Gilmore 1995; Kordopatis et al. 2011; Lee et al. 2011b). With respect to the thin disc, the thick disc stars are older and have an enhanced ratio of α-element abundances over iron ([α/Fe], e.g. Bensby et al. 2005, 2007; Fuhrmann 2008). Nevertheless, it progressively appeared that the distributions in the above mentioned physical parameters displayed significant overlaps between the thin and the thick disc populations (e.g. Bensby & Feltzing 2010). This blurred our comprehension of the interplay between the discs and challenged the classical kinematically-based definitions (Bovy et al. 2012c).

On the other hand, as discussed in Bovy et al. (2012b), defining stellar populations by abundance patterns is a better approach than the traditional kinematical criteria, because chemical abundances can correlate with disc structure, but are formally independent of it. Moreover, the identification of possible chemical evolutionary paths and/or gaps in the abundance ratios distributions can be crucial for disentangling the otherwise overlapping populations in the kinematical space.

In recent years, the number of stars analysed with spectroscopic resolution that is high enough to provide detailed chemical diagnostics has increased from a few hundred to several tens of thousands. The advent of Milky Way spectroscopic surveys and of automatised chemical analysis techniques have improved both the statistical robustness and the homogeneity of the data as a consequence. From the theoretical side, new approaches based, at least partially, on the chemical identification of disc sub-populations, such as chemical-tagging (Freeman & Bland-Hawthorn 2002) or the mono-abundance populations (Rix & Bovy 2013) methods, are opening promising pathways for constraining the Milky Way's evolutionary processes. This is also challenging our previous conception of the Milky Way disc and the way in which stellar populations can be defined.

In this context, the low-resolution ($R \sim 2000$) SEGUE spectroscopic survey has addressed the question of the thin to thick disc transition with a robust statistical approach, inside and outside the solar neighbourhood. Lee et al. (2011b) analysed ~17 300 G-type dwarfs with errors of about 0.23 dex in [Fe/H] (Smolinski et al. 2011) and 0.1 dex for [α/Fe] (Lee et al. 2011a). This was complemented by Schlesinger et al. (2012), who analysed 24 270 G and 16 847 K dwarfs at distances from 0.2 to 2.3 kpc from the Galactic plane. The Lee et al. (2011b) [α/Fe] versus [Fe/H] distribution of number densities (see their Fig. 2) already motivated the authors to chemically separate the thin and the thick disc populations, although no clear gap is observed between the two. The SEGUE data interpretations differ from authors proposing no thin-thick disc distinction (Bovy et al. 2012b) to those allowing the existence of a distinct thick disc component formed through an external mechanism (Liu & van de Ven 2012). Nevertheless, selection effects have been invoked to explain some of the distinctions between the Lee et al. (2011a) and the Bovy et al. (2012b) chemical distributions. On the other hand, the data interpretation in the sense of no thin-thick disc distinction agrees with the results of the Schönrich & Binney (2009a) theoretical study.

More recently, Boeche et al. (2013) have analysed the chemo-kinematical characteristics of 9131 giants included in the last RAVE survey data release, with available [M/H] and [α/Fe]. The RAVE survey data have a higher resolution ($R = 7500$) than SEGUE spectra, but with a wavelength range limited to the infrared Ca II triplet. The Boeche et al. (2013) analysis, based on the eccentricity-Zmax plane combined with additional orbital parameters, allowed them to identify three stellar populations that could be associated with the Galactic thin disc, a dissipative component composed mostly of thick disc stars, and the halo. Nevertheless, their thin and thick disc populations, defined with the above mentioned dynamical criteria, do not clearly separate in their [α/Fe] vs. [M/H] plane (cf. their Fig. 10).

On the other hand, recent studies of solar neighbourhood samples, analysed with high-resolution spectroscopic data, have revealed the existence of a gap in the [α/Fe] versus [Fe/H] plane (e.g Fuhrmann 2004; Reddy et al. 2006; Bensby et al. 2007). Recently, Adibekyan et al. (2013) used the stellar sample of 1111 long-lived FGK dwarf stars from Adibekyan et al. (2012) to separate and characterise the different Galactic stellar subsystems, taking the existence of this gap into account. Their [α/Fe] measurements are based on Mg, Si, and Ti averaged abundances and the typical relative uncertainties in the metallicity and [α/Fe] are about 0.03 dex. Haywood et al. (2013) derived ages of the Adibekyan et al. (2012) sample, concluding that two regimes appear in the age-[α/Fe] plane, that they identify as the epochs of the thick and thin disc formation. In the Haywood et al. (2013) scenario, the thick disc "formed from a well mixed interstellar medium, probably first in starburst, then in a more quiescent mode, over a time scale of 4–5 Gyr". They also suggest that "the youngest thick disk set the initial conditions from which the inner thin disk started to form 8 Gyr ago, at [Fe/H] in the range of (–0.1, +0.1) dex and [α/Fe] = 0.1 dex". Finally, they interpret the low-metallicity tail of the thin disc as having an outer disc origin, somewhat disconnected from the inner disc evolution. In addition, similar separations in the [α/Fe] versus [Fe/H] plane are distinguishable in the Ramírez et al. (2013) oxygen-abundance versus [Fe/H] measurements. These authors also report similar age-[α/Fe] regimes as in Haywood et al. (2013).

In summary, the increasing number of Galactic disc stars with known kinematical and chemical characteristics has emphasized the question of the continuity between the thick and the thin disc components, in structural properties, kinematics, abundances, and ages. Different authors such as Norris (1999) and Bovy et al. (2012b) have even raised the possibility of considering the Galactic disc as a single component, without a thick/thin disc distinction, analysing for instance the mass-weighted scale-height distribution of disc stars.

In this context, the GIRAFFE observations of the *Gaia*-ESO Survey (GES, Gilmore et al. 2012) offer a unique opportunity to extend the previous high-resolution studies of the solar neighbourhood to larger and more radially extended samples. In its first data release, GES already includes ~10 000 spectra ($R \sim 20\,000$ and $R \sim 16\,000$) of stars in the Milky Way field, from the halo, the thick disc, the thin disc, and the bulge. The expected final number of targets at the end of the five years of observations is ~100 000.

The present paper addresses the thick-thin disc transition as seen in the GES kinematical and chemical ([α/Fe] and global metallicity) first release data of FGK-type stars. Our point of view, when exploiting the high resolution of the GES data, is that of the chemical characterisation and definition of the disc populations (essentially identified as thin and thick discs). As a consequence, the subsequent analysis of the structural properties, kinematics, and orbital parameters will be done in the framework of the chemically defined disc populations. Section 2 describes the data sample, including the stellar parameters and [α/Fe] measurements. Section 3 presents the derivation of the

stellar distances and kinematics. Section 4 focusses on the analysis of the number density distribution in the [α/Fe] versus [M/H] plane. Then, the distributions of the distances to the Galactic plane (Sect. 5), of the azimuthal velocities (Sect. 6), the azimuthal and vertical velocity dispersions (Sect. 7), and the stellar orbital parameters (Sect. 8) are discussed in the context of a proposed thick-thin disc separation based on the chemical criteria. Section 9 presents the rotational and abundance gradients with galactocentric radius and, finally, we discuss our results in Sect. 10.

2. The GES data sample, the stellar parameters, and the [α/Fe] measurements

The present work is based on the data collected by the *Gaia*-ESO Survey during the first nine months of observations. As explained in Gilmore et al. (2012), the GES consortium has a work package structure that manages the data flows from target selection through data reduction, spectrum analysis, astrophysical parameters determination, calibration, and homogenisation to the delivery of science data for verification analysis. The general data processing is described in Gilmore et al. (in prep.).

In this paper, we analyse the iDR1 GES results for ∼5000 Milky Way disc field stars observed with the GIRAFFE spectrograph: 4534 stars observed with both the HR10 ($R \sim 19\,800$) and the HR21 ($R \sim 16\,200$) setup modes, and 394 stars with only HR10 spectra. Figure 1 shows the l and b coordinates for the lines of sight of the GES iDR1 (bulge and star clusters fields are excluded). All the targets were selected from Visible and Infrared Survey Telescope for Astronomy (VISTA) photometry. As explained in Gilmore et al. (2012), the target selection for the halo and disc targets is based on the disc/halo transition seen in the Sloan Digital Sky Survey photometry at $17 < r < 18$ and $0.2 < g - r < 0.4$. The equivalent selection from VISTA near-infrared photometry is used by GES with two main selection boxes:

- Blue box: $0.0 < J - K < 0.45$ and $14.0 < J < 17.5$ mag.
- Red box: $0.4 < J - K < 0.70$ and $12.5 < J < 15.0$ mag.

The colour boxes are shifted according to the Schlegel extinction maps (Schlegel et al. 1998). In addition, when the stellar density was not enough to fill in all the FLAMES fibers, as for high-latitude fields, the red box was extended to around $J - K < 0.85$ and $J < 17$ mag to allow for second priority fibers. The spectrum analysis has shown that the blue box has mainly selected dwarf stars with $T_{\rm eff}$ between 6500 K and 5250 K. The corresponding metallicity distribution peaks at around –0.6 dex for high-latitude fields ($|b| > 30$) and at –0.3 dex for low latitude fields. On the other hand, the red box has targeted dwarfs with $T_{\rm eff}$ between 6000 K and 4500 K and a small number of giant stars. The metallicity distribution of the red box targets is quite independent of the latitude, and it peaks around −0.4 dex. Finally, the extention of the selection boxes in the low density fields has added main sequence dwarfs with $T_{\rm eff}$ between 6000 K and 4000 K with a doubled-peaked metallicity distribution (peaks at ∼−0.8 dex and –0.3 dex). The signal-to-noise value of this second priority targets is in general lower than the main target data. As a consequence of the selection criteria, the thin disc is preferably targeted in the low latitude fields with respect to the thick disc, in a proportion of about 3:1, against about 1:1 for the high-latitude fields.

The radial velocity measurements are based on a spectral fitting technique that includes a first-guess determination of atmospheric parameters. The method is described in detail by Koposov (in prep.). Typical errors in radial velocity are of the order of 0.3 km s^{-1}. The stellar atmospheric parameters, and [α/Fe] abundances were determined by the GES work package in charge of the GIRAFFE spectrum analysis for FGK-type stars. The final recommended effective temperatures ($T_{\rm eff}$), surface gravities (log g), global metallicities ([M/H]), and [α/Fe] abundances ([α/Fe]) were estimated from the combination of three different procedures: MATISSE (Recio-Blanco et al. 2006), FERRE (Allende Prieto et al. 2006, and further developments), and SME (Valenti & Piskunov 1996, and further developments). The relative error distributions peak at 70 K for $T_{\rm eff}$, 0.10 dex for log g, 0.08 dex for [M/H], and 0.03 dex for [α/Fe]. The homogeneity of the parameters between the stars observed with HR10 and HR21 and those observed with HR10 was only verified during the GES parameters validation process. The adopted reference solar abundances are those of Grevesse et al. (2007) and the Gustafsson et al. (2008) MARCS model atmospheres were used for the analysis. For more details about the related GES parametrisation pipeline, we refer the reader to Recio-Blanco et al. (in prep.). In addition, 95% of the targets have proper motions available from the PPMXL catalogue (Roeser et al. 2010) with typical errors of 8 mas/yr.

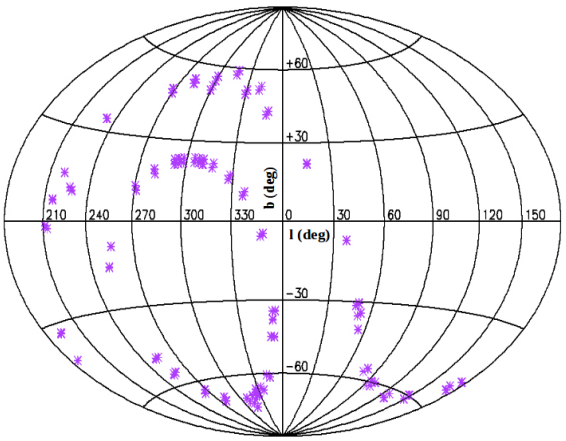

Fig. 1. l and b coordinates for the lines of sight of the GES iDR1 (bulge and star clusters fields are excluded).

Figure 2 shows the Hertzsprung-Russel diagram of the analysed sample of 4928 GES stars, colour-coded by metallicity. Dwarfs stars represent about 74% of the total sample.

2.1. The global [α/Fe] estimations

The GES [α/Fe] estimations used in this paper were determined at the same time as the stellar atmospheric parameters, by the three above mentioned groups with different methodologies (Recio-Blanco et al., in prep.). More particularly, the final GES iDR1 [α/Fe] values are the mean of the three independent determinations: the FERRE and the MATISSE estimations, based on a 4D ($T_{\rm eff}$, log g, [M/H], and [α/Fe]) grid of synthetic spectra (see de Laverny et al. 2012, for a description of the methodologies adopted for this grid); and the SME determination, based on a mean of the preliminary individual abundance estimations of Mg, Ca, Ti and Si. This global [α/Fe] is estimated in the first analysis phase, together with $T_{\rm eff}$, log g , and [M/H], and before the final GES recommended individual abundances are determined.

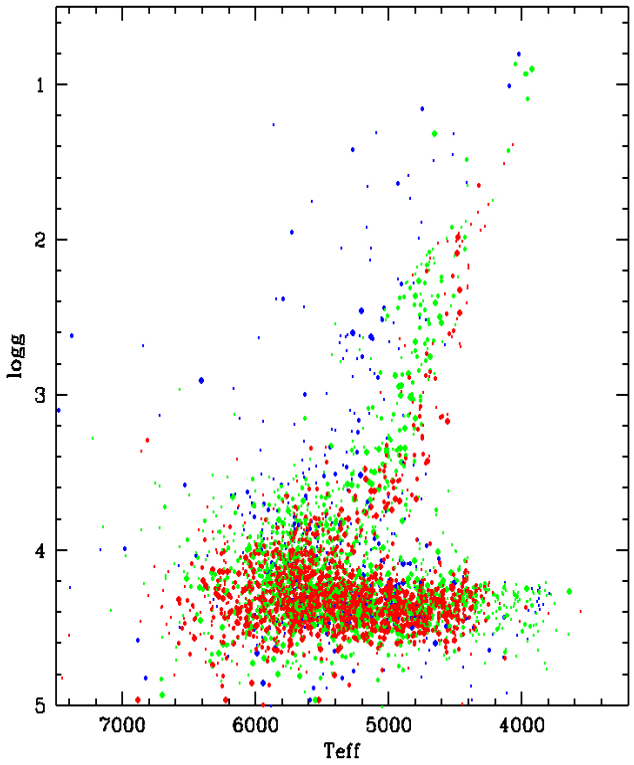

Fig. 2. Hertzsprung-Russel diagram of the selected sample of GES stars. Red points correspond to stars with [M/H] > −0.5 dex, green points are intermediate-metallicity stars (−1.0 dex < [M/H] ≤ −0.5 dex), and blue points are metal-poor objects ([M/H] ≤ −1.0 dex). To enhance the best quality data, the points size is inversely proportional to the associated errors in the atmospheric parameters.

As explained in Recio-Blanco et al. (in prep.), the final global [α/Fe] reflects the information on the α-element abundances present in the analysed wavelength ranges for each type of star and spectrum quality. This approach, similar to the SDSS/SEGUE one described by Lee et al. (2011b), estimates the overall α-elements behaviour. The relation between the GES iDR1 global [α/Fe] and the individual α-element abundances, also included in the GES iDR1 (Mg, Ca, Ti, and Si), is presented in Recio-Blanco et al. (in prep.). This analysis shows that the global [α/Fe] is dominated by the Mg abundance, with a standard deviation of the difference equal to 0.069 dex.

Finally, GES iDR1 measurements of the Fe abundance are also available, although they are not used in this paper. The relation between [M/H] and [Fe/H] has also been verified, and it is presented in Recio-Blanco et al. (in prep.). The standard deviation of the difference between [M/H] and [Fe/H] is 0.10 dex.

3. Distance estimations and kinematics

The determination of the stellar distances is based on the method presented in Kordopatis et al. (2011) and successfully applied in Gazzano et al. (2013) and Kordopatis et al. (2013b). This method projects the atmospheric parameters, $T_{\rm eff}$, log g, [M/H], and their errors on a set of isochrones, obtaining the most likely absolute magnitude of the star, given an a-priori knowledge of the lifetime spent by a star on each region of the HR diagram (i.e. main sequence stars are, statistically, more likely to be observed).

The isochrones on which the atmospheric parameters are projected are the ones of Yonsei-Yale (Demarque et al. 2004), combined with the colour tables of Lejeune et al. (1998). Using the provided interpolation code, we generated a set of isochrones with a constant step in age of 1 Gyr, starting from 1 Gyr to 14 Gyr. As far as the metallicities are concerned, the isochrones are within a range of −3.0 < [Fe/H] < 0.8 dex, constantly spaced by 0.1 dex. The α-enhancements of the isochrones have been selected in the following way, according to the typical [α/Fe] of disc and halo stars:

- [Fe/H] ≥ −0.1 dex, then [α/Fe] = 0.0 dex;
- −0.1 ≤ [Fe/H] ≤ −0.3 dex, then [α/Fe] = +0.1 dex;
- −0.4 ≤ [Fe/H] ≤ −0.6 dex, then [α/Fe] = +0.2 dex;
- −0.7 ≤ [Fe/H] ≤ −0.9 dex, then [α/Fe] = +0.3 dex;
- [Fe/H] ≤ −1 dex, then [α/Fe] = +0.4 dex.

On the other hand, in a similar approach to the one used here, Zwitter et al. (2010) have shown that adopting isochrones of different alpha abundances does not affect the distance determination significantly.

In addition to the atmospheric parameters, the $(J - K_{\rm s})$ colours are also used to obtain the most likely absolute magnitude of the star. Nevertheless, to do so, one must correct by the effect of the reddening, which is a function of the stellar distance and of the dust distribution. For that reason, we proceed in two steps. First, we compute the distances without using the colours, and we estimate the extinction at the distance of the star iteratively . Then, we apply the colour correction to the $(J - K_{\rm s})$ of the star, and re-compute the distances one final time using the de-reddened colour.

3.1. Extinction correction

The band in which we compute the distance modulus is the $J_{\rm VHS}$ band. For the brightest targets, no VHS (VISTA Hemisphere Survey) photometry is available, owing to the saturation limits of the survey, so we have adopted the 2MASS photometry, where we have $J_{\rm 2MASS} = J_{\rm VHS}$ and $K_{\rm 2MASS} = K_{\rm VHS}$. In addition, the $(JK)_{\rm ESO}$ provided by the Yonsei-Yale isochrones match the $(JK_{\rm s})_{\rm 2MASS}$ and $(JK_{\rm s})_{\rm VHS}$ very well , so no colour transformation is needed when manipulating the magnitudes from the different photometric systems (Carpenter 2001).

Once we have the absolute magnitude of the star using the Kordopatis et al. (2011) pipeline, a first estimation of the distance of the star is obtained, assuming the Schlegel et al. (1998) reddening. For the lines-of-sight with the highest reddening ($E(B-V)$ higher than 0.10 mag), we applied the correction suggested by Bonifacio et al. (2000):

$$E(B-V)_{\rm a} = 0.10 + 0.65 * [E(B-V)_{\rm sch} - 0.10], \quad (1)$$

where $E(B-V)_{\rm sch}$ is the Schlegel et al. (1998) reddening, and $E(B-V)_{\rm a}$ the adopted one. The extinction in the $(JK_{\rm s})$ bands is then estimated using the following equations from McCall (2004):

$$A_J = 0.819 * E(B-V)_{\rm a} \quad (2)$$

$$A_{K_{\rm s}} = 0.350 * E(B-V)_{\rm a}. \quad (3)$$

By applying the above extinction to the apparent magnitude and deriving the line-of-sight distance, we over-estimate the distance of the stars because the Schlegel et al. (1998) reddening is a value integrated along the entire length of the line-of-sight. We thus compute the following correction factor to apply for the Schlegel reddening, assuming an exponential disc of dust:

$$E(B-V)_{\rm corrected} = E(B-V)_{\rm a} * \left(1 - {\rm e}^{\frac{-|D\ \sin(b)|}{h_{\rm dust}}}\right), \quad (4)$$

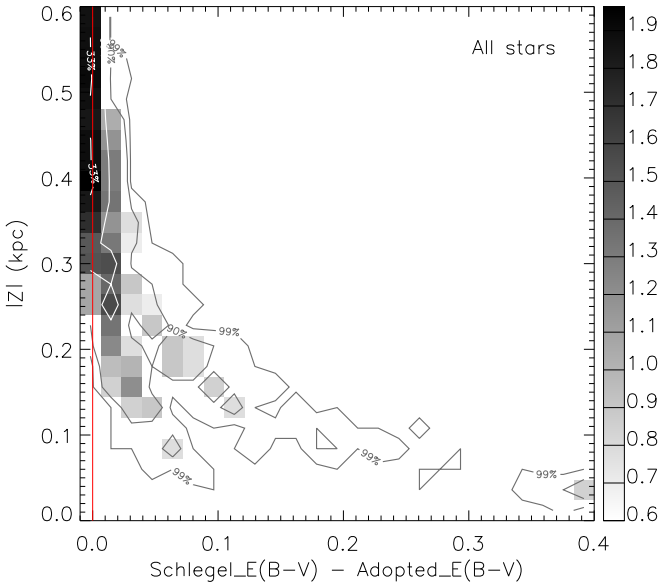

Fig. 3. Reddening correction computed for each star depending on its line-of-sight distance, as a function of its distance from the Galactic plane Z. The grey-scale colours represent the star counts in $\log_{10}(N)$. The contour lines contain 33%, 66%, 90% , and 99% of the stars. As expected the corrections made to $E(B-V)_a$ are only for the stars located closer than 400 pc from the Galactic plane.

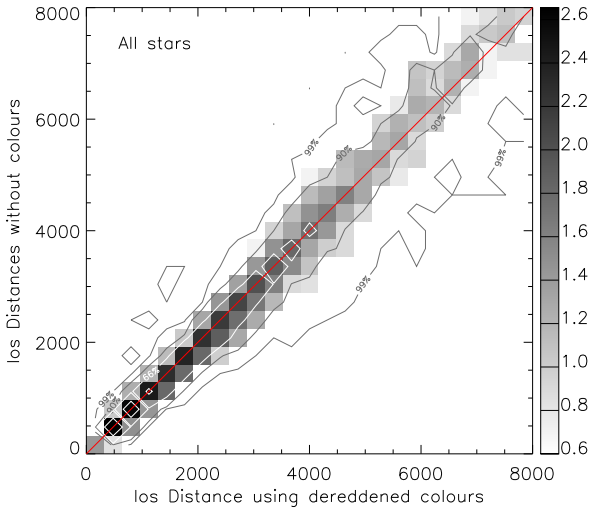

Fig. 4. Change in the line-of-sight distance estimates when using only the effective temperature, surface gravity, iron abundance (y-axis), and the previously mentioned atmospheric parameters in combination with the $(J - K_s)$ colour (x-axis). The differences are mainly noticeable for the most distant stars. The colour-coding and the contour lines are the same as in Fig. 3

where $h_{\rm dust}$ = 125 pc is the scale height of the disc of dust that causes the reddening (Misiriotis et al. 2006), D the line-of-sight distance, and b the Galactic latitude of the target.

Once the correction have been applied, we compute the distance to the star again, and following Ruchti et al. (2011), we repeat the above step iteratively until the difference between two consecutive distance estimations is less than 2%. For the few stars that lie within the dust lane, no more than four iterations are needed until convergence. The adopted reddening correction, as a function of the distance from the Galactic plane, is shown in Fig. 3.

Once the final extinctions have been computed, the dereddened $(J-K_s)$ colour of the star is estimated, and the pipeline is run to estimate the absolute magnitude of the star, using this time the $(J - K_s)$ colours. The effect on the derived line-of-sight distances is plotted in Fig. 4. These distances are the ones that are used below (see for instance Fig. 14).

3.2. Errors in the line-of-sight distances

To estimate the errors in the derived distances, we performed 5000 Monte-Carlo realisations on the errors on the distance modulus. Those errors include the error on the derived absolute magnitude J (which takes the errors in $T_{\rm eff}$, log g, [M/H] into account), and the error on the apparent J and K_s magnitudes. The uncertainty in the atmospheric parameters is considered when computing the absolute magnitude, in the same fashion as described in Kordopatis et al. (2011), i.e. by estimating the dispersion of the weighted absolute magnitude of the stars on the isochrones. The parameter dominating the error in the distances is $T_{\rm eff}$ for main sequence stars and log g for giants.

Figure 5 shows the cumulative histogram of the derived distance errors, for the entire sample and for a sub-sample with signal-to-noise ratios higher than 15 and errors in $T_{\rm eff}$ and log g lower than 400 K and 0.5 dex, respectively. There, σ_D is the

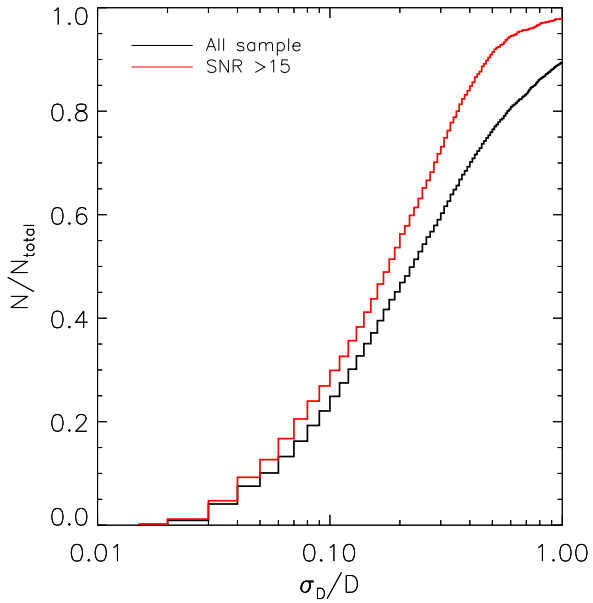

Fig. 5. Cumulative histogram of the derived distance errors, for the entire sample (black line) and for stars with $S/N > 15$ (red line).

inferred error bar when the above factors are taken into account. As shown in Fig. 5, 45% of the total sample has $\sigma_D/D < 20\%$ and 80% has $\sigma_D/D < 50\%$. These values increase to 55% and 90% for the selected sub-sample of $S/N > 15$ (2107 stars). In addition, Figs. 6 and 7 show the dependences of the distance errors on the metallicity and on the distance value itself, for stars with $S/N > 15$. The final errors in positions for the individual stars are included in Table 1.

3.3. Validation of the distances

We verified the accuracy of our results by evaluating the distances found for the globular cluster (GC) stars that were observed and labelled as such by GES. The reference distances

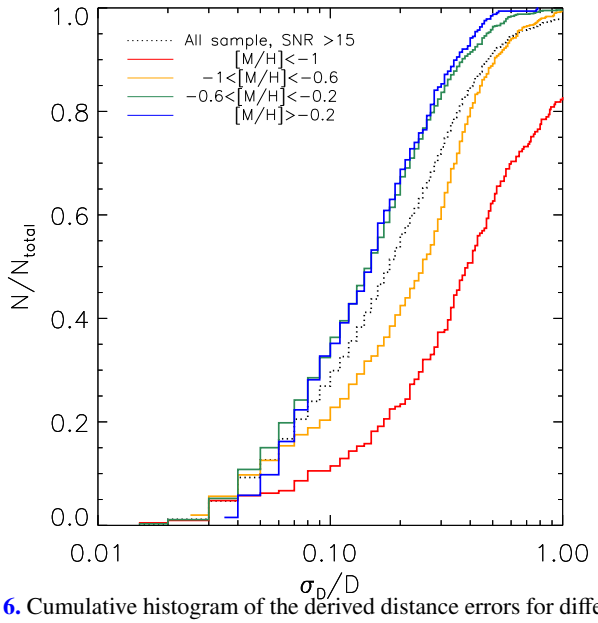

Fig. 6. Cumulative histogram of the derived distance errors for different metallicity bins, for stars with $S/N > 15$.

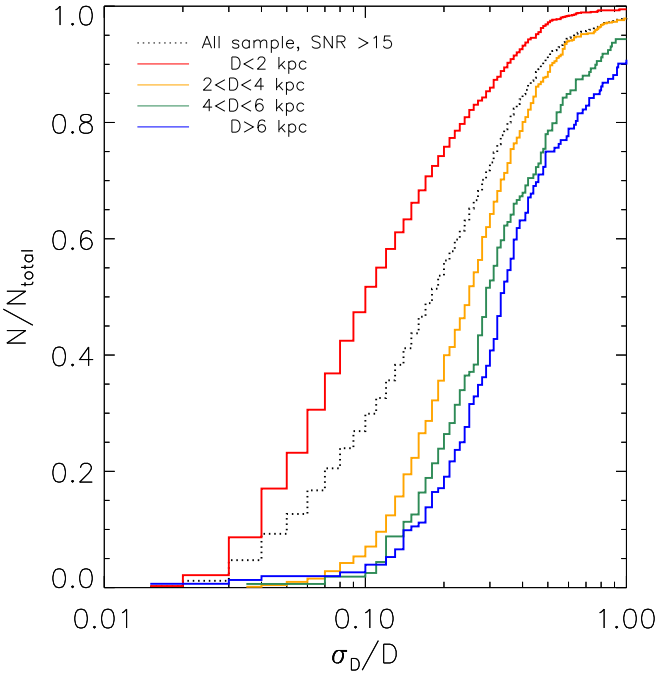

Fig. 7. Cumulative histogram of the derived distance errors for different distance bins, for stars with $S/N > 15$.

are the ones from Harris (1996), in the updated version (December 2010) of the catalogue[1], summarised in Table 2. To remove foreground contamination, in addition to using the GES labels, we have rejected all the targets that were outside the 3σ of the velocity dispersion of the GC (an arbitrary value of $\sigma = 10$ km s^{-1} was adopted when this information was not available) and had iron abundances lower or greater than 0.5 dex of the mean cluster value (see Table 2).

Figure 8 shows the histogram of the difference between the derived distance, D, and the reference one, $d_{\rm Harris}$, normalised by the estimated individual error on the distances σ_D (obtained from our pipeline). The error bars indicate the Poisson noise, i.e. the square root of the stars for each bin. Three stars were removed from the figure because they were lying at $(D - d_{\rm Harris})/\sigma_D = -581$, -293, and -289 and were considered as contaminators. In the case where our analysis is bias free and the errors correctly estimated, the histogram of Fig. 8 is supposed to be Gaussian-centred on zero and of unit dispersion. We can see that this is the case, validating our approach in that way. More precisely, once the three contaminators have been removed, we find a distribution centred at 0.20 and a standard deviation of 1.14. The mean value of the $(D-d_{\rm Harris})/\sigma_D$ distribution corresponds to a bias in the estimated distances ($(D-d_{\rm Harris})/D$) of less than 5%. The value of the sigma indicates an underestimation of the errors of ~14% with respect to the differences between the literature values and the ones derived in this work. However, we would like to stress that the Harris- errors on the distance of the GCs could probably explain most of this difference. On the other hand, the slight asymmetry of the histogram comes from the measurements of NGC 4 372, which has also the lowest metallicity, hence the atmospheric parameters with the largest uncertainties. In addition, it is worth noticing that the GES iDR1 globular cluster targets are giant stars, while the majority of the observed field stars are main sequence objects. Although GES is a magnitude-limited sample, 80% of the targets are placed at smaller distances than the above analysed GCs.

Finally, it is worth mentioning that for dwarf stars, as explained in Recio-Blanco et al. (in prep.), a degeneracy between $T_{\rm eff}$ and log g appears progressively, as $T_{\rm eff}$ decreases, starting around $T_{\rm eff} \sim 5000$ K. This degeneracy gives rise to a negative bias (stars may appear cooler and at lower gravities). We explored the consequence on the derived distances on this degeneracy, taking into account that the distances are calculated after the projection of the atmospheric parameters on the isochrones. In the corresponding cool part of the main sequence, $T_{\rm eff}$ is the main parameter influencing the absolute magnitude determination, since the isochrones points of different ages and metallicities are all tightly located in the HR diagram. In addition, as the slope of the isochrones is very low, the determined distances are not very sensitive to errors in $T_{\rm eff}$. Moreover, the projection of the determined parameters on the isochrones, for the distance determination, corrects both $T_{\rm eff}$ and log g. This correction is close to the bias for stars with $T_{\rm eff} > 4500$ K. For cooler stars ($4500 > T_{\rm eff} > 4200$ K), the residual bias in $T_{\rm eff}$, after the isochrone projection, is around 100 K. This error in $T_{\rm eff}$ implies around 6% to 7% of the distance error, depending on the metallicity. For this work, the selected stellar sub-sample of iDR1 (cf. Sect. 4) only contains 3% of stars cooler than 4500 K in the thin disc sequence, and 2% in the thick disc one. Therefore, in the worst case, a bias of only ~7% in distance, well inside the typical errors of the sample, can appear for about 2% to 3% of our final sample.

3.4. Derivation of Galactocentric velocities

From the derived line-of-sight distances, the 3D Galactic positions are obtained for all the analysed stars (assuming $R_\odot = 8$ kpc and $Z_\odot = 0$ pc, see Reid 1993). The derived values together with their associated errors are reported in Table 1. Once the 3D Galactic positions are obtained, the galactocentric radial, azimuthal, and vertical velocities are computed using the PPMXL proper motions, and the equations from the appendix of Williams et al. (2013). We have used $(U_\odot, V_\odot, W_\odot) = (11.1, 12.24, 7.25)$ km s^{-1} (Schönrich et al. 2010) and the local standard of rest (LSR) is at $V_{\rm LSR} = 220$ km s^{-1}. The obtained galactocentric velocities are reported in Table 1.

[1] http://www.physics.mcmaster.ca/~harris/mwgc.dat

Table 1. Derived stellar distances (D), positions (in the R and Z coordinates), and kinematics (radial, azimuthal, and vertical velocities), plus their associated errors (ΔD, ΔR, ΔZ, ΔV_R, $\Delta V_{\rm phi}$, and ΔV_Z).

ID	D	ΔD	R	ΔR	Z	ΔZ	V_R	ΔV_R	$V_{\rm phi}$	$\Delta V_{\rm phi}$	V_Z	ΔV_Z
gir00184577-4700293	0.819	0.081	7.783	0.021	–0.766	0.076	17	37	253	37	–24	13
gir00184695-4659371	2.113	0.113	7.451	0.028	–1.975	0.106	–12	97	203	100	25	37
...	...	...	...	...	...	...	...	...	...	...	...	...

Table 2. Adopted globular cluster parameters: line-of-sight (los) distance, reddening, iron abundance, radial velocity and central velocity dispersion (from Harris 1996, updated version of the catalogue, Dec. 2010).

Cluster	Los distance (kpc)	$E(B-V)$ (mag)	[Fe/H] (dex)	$V_{\rm rad}$ (km s^{-1})	$\sigma V_{\rm rad}$ (km s^{-1})	Derived los distance (kpc)
NGC 5 927	7.7	0.45	–0.49	–107.5		8.9 ± 3.3
NGC 1 851	12.1	0.02	–1.18	320.5	10.4	11.3 ± 4.1
NGC 2 808	9.6	0.22	–1.14	101.6	13.4	9.4 ± 3.1
NGC 4 372	5.8	0.39	–2.17	72.3		8.1 ± 3.1

Notes. The two last columns show the derived distances with their associated errors (quadratic sum of the standard deviation of the members distances and their median individual errors).

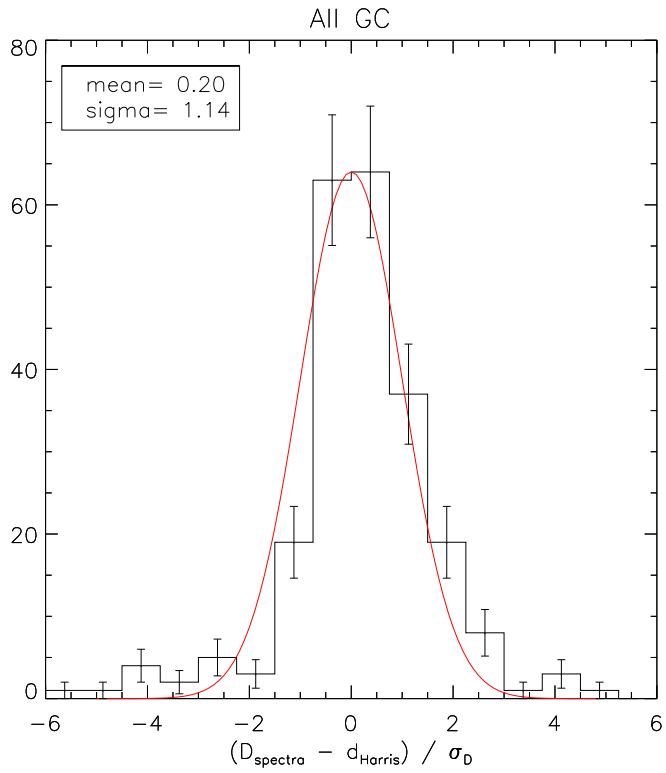

Fig. 8. Histogram of the error distribution for all the stars selected as belonging to the globular clusters observed by GES. The red Gaussian is not a fit of the histogram but represents the unit Gaussian that should follow perfect bias-free measurements with correct error estimations. A very satisfactory result is obtained, with an estimated bias of ~5% and a standard deviation of ~14%.

3.5. Error estimation in velocities

To evaluate the errors on the stellar velocities, we performed 5000 Monte-Carlo realisations, considering that the proper motions, the radial velocities, and the line-of-sight distances are independent. Depending on the galactic coordinates (l, b) of a star, the uncertainties on the distances, the proper motions and the radial velocities will affect the 3D-velocity estimations in a different manner. Typically, the dominant source for the uncertainty comes from the errors in proper motions (typical errors of 8 mas/yr, see Sect.2), whereas the errors on the radial velocities (typically 0.3 km s^{-1}) in general have a negligible effect. As an example, for a given star at 1 kpc in $290 < l < 340$ and $10 < b < 30$, the contribution to the 3D-velocity uncertainties will be of 5−10 km s^{-1} for an error of 10−20% on the distance and of 15−30 km s^{-1} for an error of 5−10 mas/yr on the proper motions. The final errors in kinematics for the individual stars are included in Table 1.

4. Chemical characterisation of the thin and thick discs

Thanks to their high resolution, the GES spectra offer an exceptional opportunity to characterise the distribution of disc stars in the [α/Fe] versus [M/H] plane, with a robust enough statistical analysis and rather low abundance errors. To this purpose, we have first selected sub-samples of stars with progressively higher errors in the abundance determination. This allows, on the one hand, to find the balance between number statistics and abundance accuracy, and on the other, to test the effects that low numbers of stars and high measurement errors could have on the characterisation of the stellar populations.

Figure 9 shows the distribution of stars in the [α/Fe] versus [M/H] plane for four progressively larger sub-samples with increasingly higher error limits in the abundance determination. Table 3 shows the maximum errors and S/N limits considered for each of the analysed sub-samples. In addition, Fig. 10 presents the same [α/Fe] versus [M/H] distributions in a contour levels form, for a complementary illustration.

The well-known decreasing evolution of [α/Fe] with metallicity is present in all the panels, within the expected values for disc stars. In addition, two sequences separated by a low-density region can be identified: the thick disc one in the high-α regime and the thin disc one in the low-α regime (see below for the selection criteria). Both sequences overlap in metallicity from about –0.8 dex to –0.3 dex. For the last sub-sample of 1952 objects, the increase in the scatter of the measurements blurs the chemical separation, although not completely.

First, as shown in Fig. 11, we have studied the position of the low-density region along the [α/Fe] vs. [M/H] plane, thanks to the analysis of the [α/Fe] distribution in four intervals of

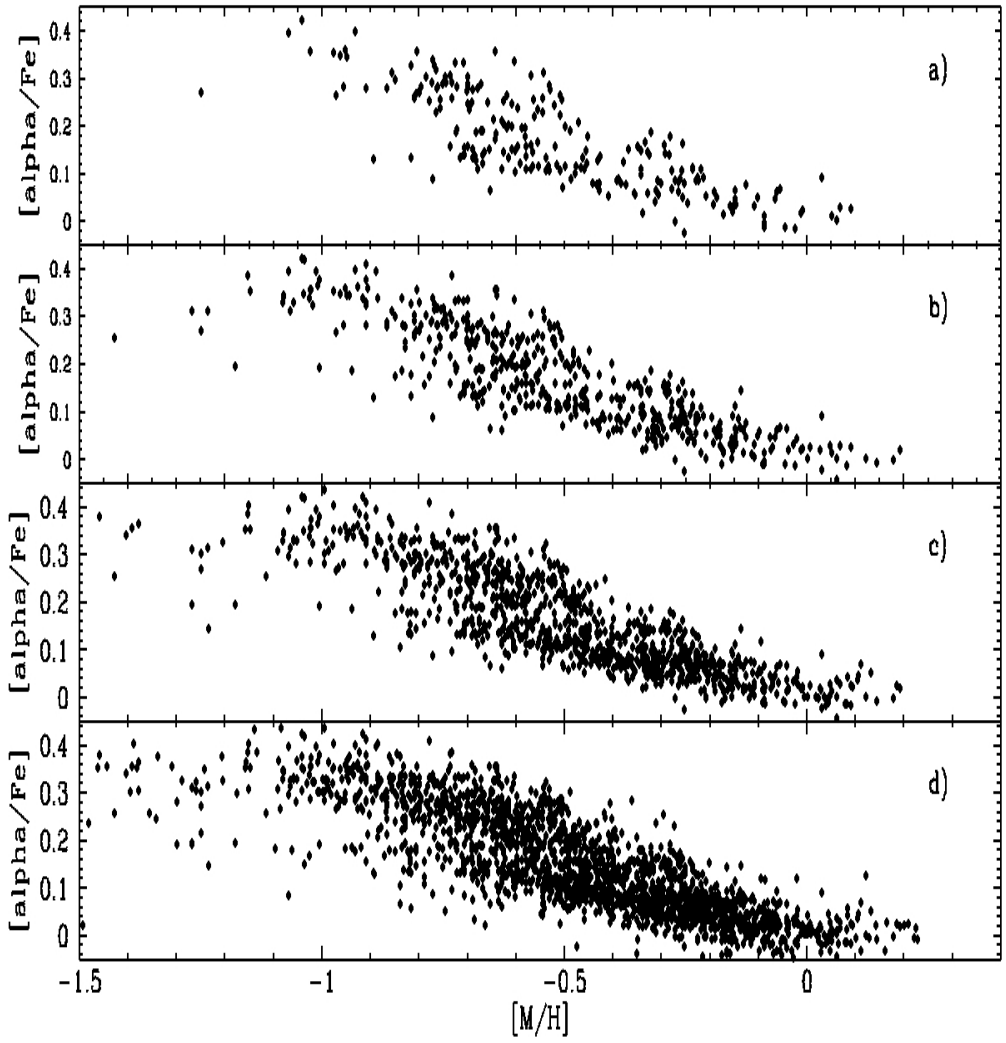

Fig. 9. α-elements over iron abundance as a function of metallicity for four different sub-samples of stars with increasing errors in the abundance determination. Panel **a)** shows the results for stars with errors in [M/H] and [α/Fe] smaller than 0.07 dex and 0.03 dex, respectively (209 stars). Panel **b)** shows the results with errors smaller than 0.09 dex and 0.04 dex in [M/H] and [α/Fe] (505 stars). Panel **c)** illustrates the values for 1008 stars with errors smaller than 0.15 dex and 0.05 dex, respectively. Finally, panel **d)** shows all the stars with errors in $T_{\rm eff}$ lower than 400 K, errors in log g lower than 0.5 dex and a spectral S/N higher than 15 for the HR10 configuration (1952 stars).

Table 3. Maximum errors allowed in the different considered sub-samples of stars.

Sub-sample id	Max error $T_{\rm eff}$ (K)	Max error log g (dex)	Max error [M/H] (dex)	Max error [α/Fe] (dex)	HR10 S/NR limit	Number of stars
a	400	0.50	0.07	0.03 dex		209
b	400	0.50	0.09	0.04 dex		505
c	400	0.50	0.15	0.05 dex		1008
d	400	0.50	–	–	15	1952
e	400	0.50	0.15 ([M/H] > −1)	0.05 ([M/H] > −1)	15	1016
			0.20 ([M/H] < −1)	0.08 ([M/H] < −1)	15	

metallicity. The largest sub-sample of stars in Fig. 11 (panel d of Fig. 9) was used for this purpose. The identified position of the gap in the [α/Fe] vs. [M/H] plane will be used in the following as the separation criterion between the thick and thin disc populations for further analysis. This low-density region is found, after a visual examination of the histograms, at [α/Fe] = 0.13, 0.19, 0.21, and 0.22 dex for the four central considered [M/H] intervals in Fig. 11.

Then, to more precisely characterise the thick and thin disc populations previously defined, and to take into account of the natural increase in the abundance measurement errors for metal-poor star's spectra (Recio-Blanco et al., in prep.), we defined a new sub-sample of objects, hereafter called *e* (cf. Table 3). This new sub-sample contains all stars with errors smaller than 0.15 dex and 0.05 dex in [M/H] and [α/Fe], respectively for [M/H] > −1 dex, plus metal-poor stars ([M/H] < −1), with allowed errors as large as 0.2 dex in [M/H] and 0.08 dex. The final

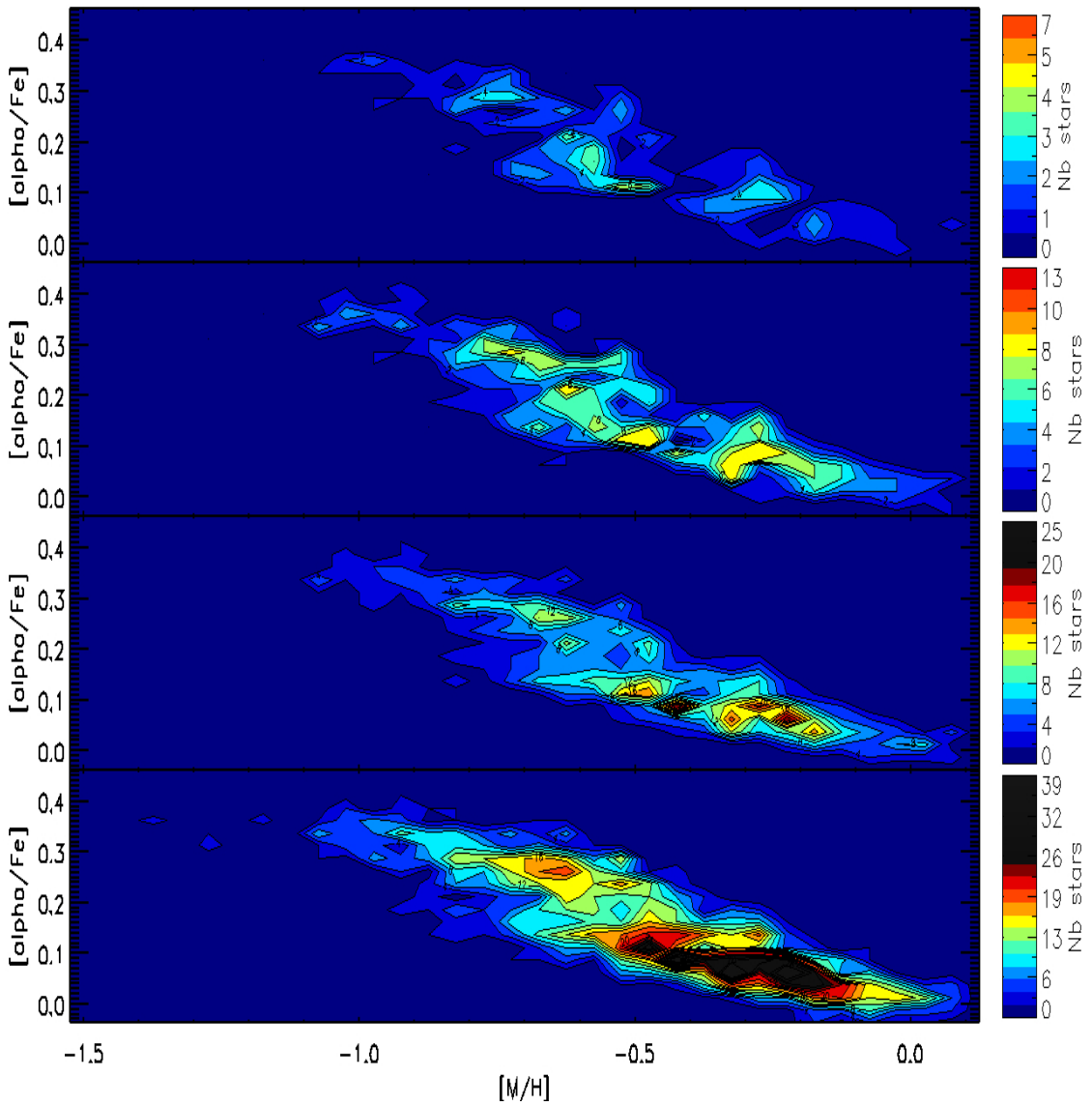

Fig. 10. Contour plots of the [α/Fe] versus [M/H] distributions of Fig. 9.

sample is shown in Fig. 12 and contains 1016 stars. A black line (based on the low-density regions defined in Fig. 11) is plotted in Fig. 12 to identify the separation between the thick and thin disc sequences. Figure 13 shows the Hertzsprung-Russel (HR) diagram of this selected sub-sample *e*. The red and blue points correspond to stars in the defined thin and thick disc sequences, respectively.

The thick disc sequence (filled circles in Fig. 12) seems to extend from [M/H] = −1.0 dex and [α/Fe] = 0.35 dex to about [M/H] = −0.25 dex and [α/Fe] = 0.1dex, decreasing linearly with a slope of about –0.30. We also considered metallicity bins of 0.2 dex and calculated the dispersion in [α/Fe] for each bin. The resulting mean [α/Fe] dispersion is 0.042 dex. This can be compared to the mean error in [α/Fe] that is equal to 0.03 dex. On the other hand, the thin disc sequence (open circles), seems to be present from about [M/H] = −0.8 dex and [α/Fe] = 0.18 dex to about [M/H] = 0.2 dex and [α/Fe] = 0.0 dex, decreasing with a slightly milder slope of about –0.20.

In addition, a high-α metal-poor population is also visible in our data, well above the Galactic plane (see Sect. 5), and occupying a flat sequence from [M/H] ∼ −1.0 dex down to the lowest sampled metallicities (filled triangles in Fig. 12). The mean [α/Fe] value of these halo stars is around 0.35 dex. This high-α metal-poor sequence could be identified with the classical high-α halo sequence or, at least partially, with the metal-weak thick disc population (e.g. Ruchti et al. 2011; Kordopatis et al. 2013a). Moreover, in the same metal-poor metallicity regime ([M/H] values lower than ∼–0.9 dex), a metal-poor low-α sequence seems to exist (asterisks in Fig. 12). After an individual inspection of these low-α metal-poor stars spectra, most of them have S/N higher than 25 in the HR10 setup, and have thus reliable [M/H] and [α/Fe] measurements. When only the lower error measurements are considered (stars with errors smaller than 0.05 dex in [α/Fe] and 0.15 dex in [M/H] and S/N for the HR10 spectra higher than 20), the low-α metal-poor stars represent about 10% of the observed stars with [M/H] values lower than ∼–0.9 dex. These stars could confirm the low-α metal-poor halo stars first observed by Nissen & Schuster (2010), and also reported by Nissen & Schuster (2011), Schuster et al. (2012), Adibekyan et al. (2012), and Ishigaki et al. (2013). On the other hand, the possible link between those objects and the metal-weak thick disc population (e.g. Morrison et al. 1990; Carollo et al. 2010; Kordopatis et al. 2013b) seems to be ruled out by their low [α/Fe] ratios, since metal-weak thick disc stars are reported to

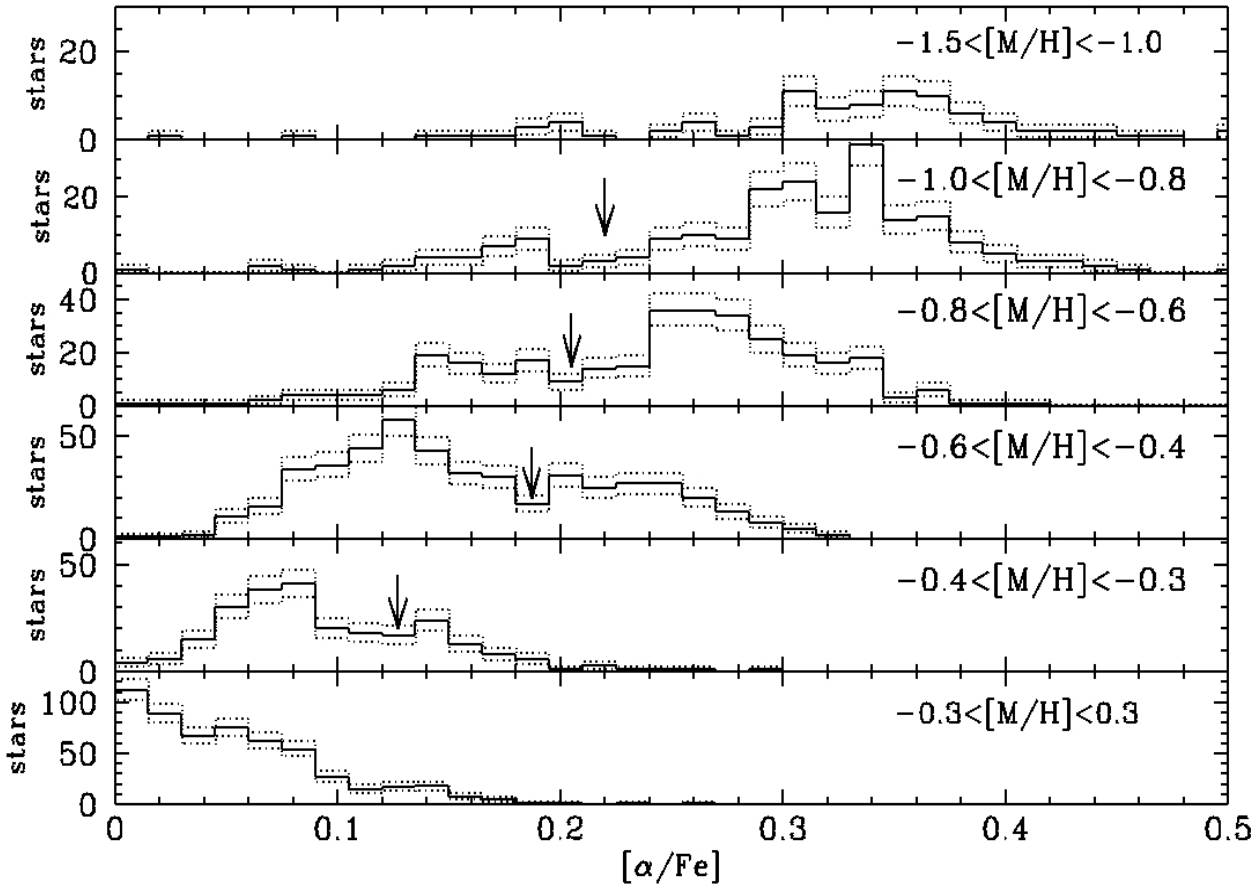

Fig. 11. Distribution of [α/Fe] values in six intervals of metallicity for the selected sub-sample (d) of Fig. 9. Error bars, corresponding to Poisson uncertainties, are given by the dotted lines. The position of the low-density region separating the thick and the thin disc sequences is marked with an arrow.

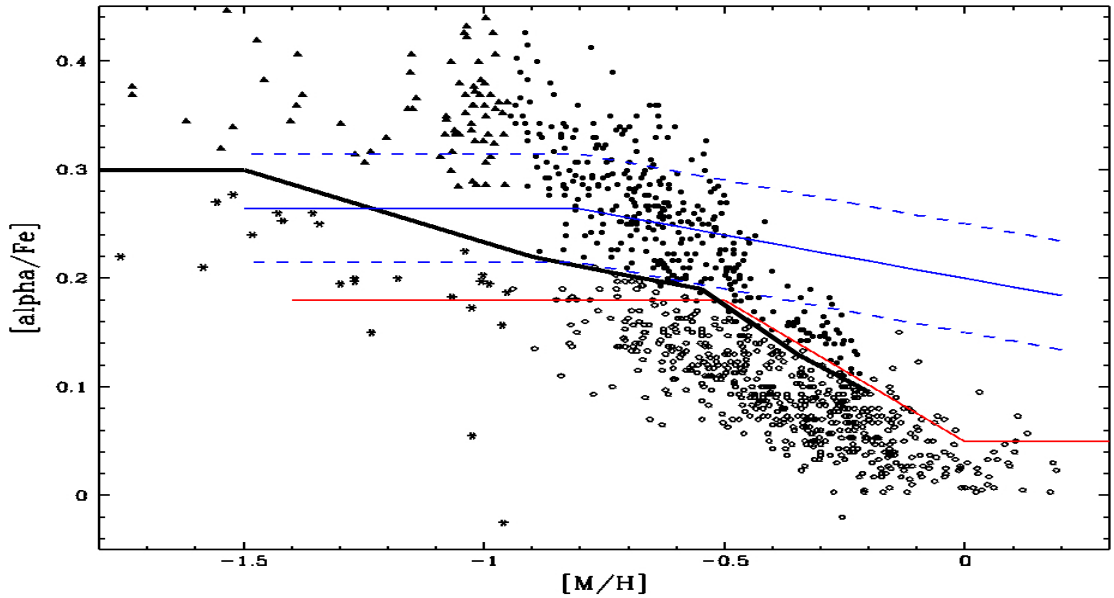

Fig. 12. α-elements over iron abundance as a function of metallicity for sub-sample *e*. Filled dots are thick disc sequence stars, open circles are thin disc sequence objects. Metal-poor stars ([M/H] < −1.0) are marked with filled triangles and asterisks, depending on whether their [α/Fe] are in the high-α or the low-α regime. The black line shows the proposed division between the thin and thick disc sequences in agreement with Fig. 11. The red line shows the separation proposed by high-resolution analysis of Adibekyan et al. (2012) for the solar neighbourhood. The blue solid line is the separation proposed by Lee et al. (2011b) from low-resolution SEGUE data and the two dashed lines indicate their dividing points for the thin and the thick disc stars to avoid misclassifying stars.

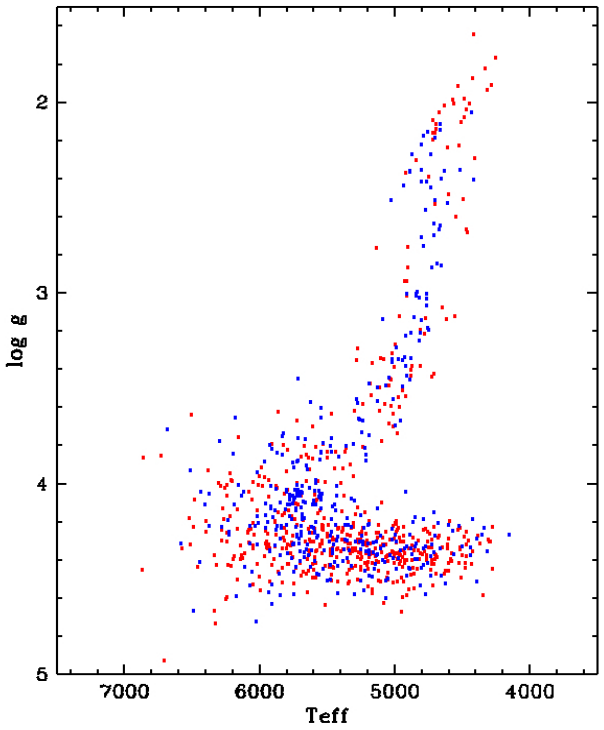

Fig. 13. Hertzsprung-Russel diagram of the selected sub-sample *e*. Red and blue points correspond to stars in the defined thin and thick disc sequences, respectively.

have [α/Fe] $\sim$ 0.3 dex (Ruchti et al. 2011). As a complementary description of these stars, the individual element abundances of these stars are analysed in Mikolaitis et al. (in prep.).

4.1. Comparison with literature studies

First of all, we compared the spatial distribution of the analysed targets with those of previous spectroscopic studies of large numbers of disc stars with available measurements of the [α/Fe] ratio, as is the case of the Lee et al. (2011b) and Adibekyan et al. (2012) analyses. We recall that the former is a low-resolution study of stars with Galactic radius in the range 7−10 kpc, and the latter is a high-resolution analysis of solar-neighbourhood stars, located at a maximum distance of about 600 pc from the Sun. Figure 14 shows the location of the GES targets analysed in this paper (*e* sub-sample of Fig. 12), in vertical distance to the Galactic plane and radial cylindrical Galactic coordinate R. To understand how many of the targets are outside the solar neighbourhood, the points are colour coded by distance. As expected from the photometric target selection, 90% of the stars are at greater distances than D = 600 pc from the Sun (i.e. much further than the Adibekyan et al. (2012) sample, comprised mainly of stars within 50 pc).

Regarding the thin to thick disc separation in the [α/Fe] vs. [M/H] plane, the above identified gap agrees with the separation seen in the Adibekyan et al. (2012) data. Figure 12 shows the Adibekyan et al. (2012) division, with three segments, which can be compared to our proposed separation. Both lines are compatible, with very small differences probably due to possible offsets in the abundance measurements between the GES analysis and the Adibekyan et al. (2012) one, or to a possible adjustment between the [M/H] and the [Fe/H] abundances. On the other hand, the Lee et al. (2011b) analysis proposes a division line with a shallower slope as illustrated in Fig. 12. Two lines indicate their dividing points for the thin and the thick disc stars, to avoid the misclassification of stars. We see that the lower dashed line allows selecting thin disc stars in fair agreement with both our selection and the Adibekyan et al. (2012) one. However, the upper dashed line excludes an important part of the thick disc sequence with intermediate and low [α/Fe] values, even if a bias between our [α/Fe] measurements and the Lee et al. (2011b) ones could exist. This could come mainly from the identification of the metal-rich part of thick disc, which would be more difficult to separate from the thin disc from low-resolution data, due to the small differences in the [α/Fe] values.

Furthermore, the difference in slope observed in our sample between the thin and the thick disc sequences seems to agree with the Haywood et al. (2013) analysis of Adibekyan et al. (2012) data, which already points out an iron enrichment of the thin disc that is lower than the thick disc one.

Finally, concerning the metal-rich end of the thin disc, no α-rich metal-rich stars are observed in our sample or in the Lee et al. (2011b) one, contrary to the results of Adibekyan et al. (2011) and Gazzano et al. (2013) and Boeche et al. (2013), which are restricted to, or predominantly at, shorter distances from the Sun. Furthermore, we note here that the number of stars with [M/H] higher than −0.1 dex is rather small in our sample, compared to the previously mentioned nearby studies.

5. Distribution of distances to the Galactic plane

As already mentioned in the Introduction, the thin and the thick discs are characterised by different scale heights. To explore the transition between these two populations, keeping their chemical separation in the [α/Fe] vs. [M/H] plane in mind as described in the above section, we have analysed the distribution of the derived distances to the Galactic plane (from the absolute values of the Galactic Z coordinate) for the target stars.

The left-hand panel of Fig. 15 shows a 3D view of the distance to the Galactic plane, in the Z-axis, as a function of [M/H] and [α/Fe], for the analysed stars (sub-sample *e* of Fig. 12). This illustration is complemented, in the right-hand panel, with a grey scale-coded 2D plot of the distribution of Z values in the [α/Fe] vs. [M/H] plane. The red line shows the separation between the thick and the thin discs sequences, defined in Sect. 4 (cf. Fig. 12). We point out that the possible halo stars discussed in the previous section are not shown in Fig. 15, because of the few objects found in each bin.

Regarding the thick disc population, the mean distances to the Galactic plane seem to decrease along the sequence from the metal-poor end to the metal-rich one:

- Z $\sim$ 1.5 kpc at [M/H] $\sim$ −0.9 dex and 0.28 < [α/Fe] < 0.40 dex;
- Z $\sim$ 1.2 kpc at [M/H] $\sim$ −0.5 dex and 0.21 < [α/Fe] < 0.30 dex;
- Z $\sim$ 0.8 kpc at [M/H] $\sim$ −0.3 dex and 0.12 < [α/Fe] < 0.25 dex.

Therefore, as the metallicity increases, the thick disc seems to lie in thinner and thinner layers. On the other hand, the distribution of vertical distances to the plane with respect to the Galactocentric radial distance is not perfectly homogeneous (cf. Fig. 14). More particularly, our sample is dominated by stars further away from the Galactic plane in the inner parts of the disc with respect to the typical heights probed in regions outside of

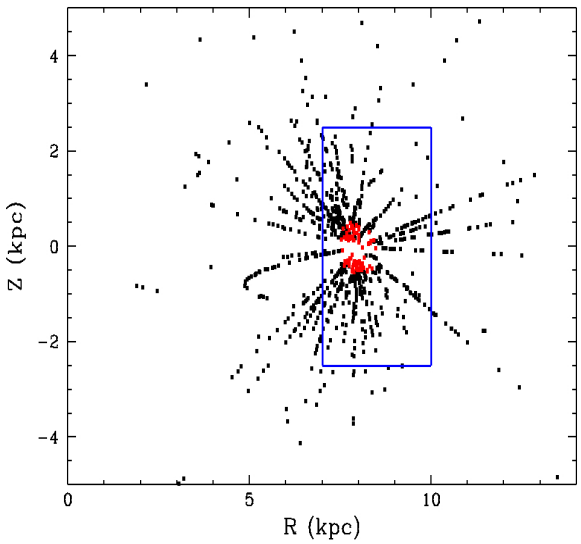

Fig. 14. Target's location, for sub-sample *e* of Fig. 12, in vertical distance to the Galactic plane (Z) and radial cylindrical Galactic coordinate (R). Red points indicate the stars with a distance value lower than 600 pc from the Sun (10% of the sample). The blue rectangle shows the maximum R and Z values of the Lee et al. (2011b) analysis of SEGUE data.

the solar radius. Thus, different Z heights can be representative of different ranges in R, and, if there were significant metallicity variations with respect to R, this would present as a variation in metallicity with height. However, as later explained in Sect. 9.2, our data show a flat distribution of [M/H] and [α/Fe] with galactocentric radius for the thick disc. Therefore, the gradient of Z that appears along the thick disc sequence in the [M/H] vs. [α/Fe] plane for increasing [M/H] values should be a real effect not caused by sampling.

On the other hand, the thin disc sequence shows a constant value of the mean distances of its stars to the Galactic plane of $Z \sim 0.5$ kpc from the metal-poor side ([M/H] ~ -0.8 dex) to the metal-rich one ([M/H] ~ 0.3 dex). Again, this conclusion should not be influenced by the spatial coverage of the studied sample, even though the thin disc has a metallicity gradient with respect to R (cf. Sect. 9.2). This is because the thin disc Z range is fairly homogeneously covered at the full range of Galactocentric radius, and, in particular, the mean Z value of the stars in the thin disc sequence does not present any clear trend with R.

As a consequence of the above conclusions, the transition from the thick disc sequence to the thin disc one in the [α/Fe] vs. [M/H] plane implies a steeper change in the mean Z distances at [M/H] around –0.8 dex than around –0.3 dex. This coincides with the fact that the chemical separation between both sequences (by a gap or a lower density region) seems clearer in the metal poor regime than in the metal rich one.

Finally, we point out that, as expected, there is a correlation between the Z distances and the associated errors, with larger errors for stars that are further from the plane. More particularly, the stars at the metal-poor high-alpha end ([M/H] around –1.0 dex) have errors around 0.45 kpc, while at [M/H] around –0.7 dex the error is about 0.20 kpc for the thick disc stars and around 0.075 kpc for the thin disc. Nevertheless, while the stars that are further from the plane have larger absolute distance errors, the percent error is actually smaller, as indicated in Figs. 6 and 7.

6. Distribution of rotational velocities

The distribution of the cylindrical rotational velocities, V_Φ, in the [α/Fe] vs. [M/H] plane is shown in Fig. 16. The rotational velocities of the stars located in the thick disc sequence have a mean value of $V_\Phi = 176 \pm 16$ km s^{-1}, and those in the thin disc have a mean $V_\Phi = 208 \pm 6$ km s^{-1}. In addition, for the thick disc, the V_Φ values seem to progressively increase from the metal-poor α-rich end (with $V_\Phi \sim 150$ km s^{-1}) to the metal-rich α-poor one ($V_\Phi \sim 190$ km s^{-1}), reaching values close to the thin disc ones.

On the other hand, a correlation between rotational velocity and metallicity is observed for both the thin and the thick disc stars, although with opposite signs. To exploit the availability of both [α/Fe] and [M/H] for our sample, we decided to analyse the correlation of rotational velocity, taking both chemical abundance parameters into account. To this purpose, and as illustrated in Fig. 17, we used the mean values of the rotational velocity for different bins of 0.05 dex in [α/Fe] and 0.20 dex in [M/H] to derive its dependence with metallicity. The chosen bin lengths are higher than the mean errors in [α/Fe] and [M/H] (0.03 dex and 0.08 dex, respectively), but they allow us to have a robust statistics per bin (a mean of 64 stars for the thin disc sequence and 34 stars for the thick disc one).

First, all the bins along the thin and thick disc sequences were considered. For the thin disc stars, we find a gradient of Galactic rotation with metallicity of -17 ± 6 km s^{-1} dex^{-1}. We checked the possible influence of the wide range of sounded galactocentric radius on the derived gradient by splitting the sample in two: stars inwards ($R < 8$ kpc) and outwards ($R > 8$ kpc) of the solar radius. The resulting values of the gradient are -20 ± 13 and -22 ± 9 km s^{-1} dex^{-1}, suggesting that the derived slopes are not indirectly created by radial gradients in metallicity. For the thick disc population, we find a positive gradient of 43 ± 13 km s^{-1} dex^{-1}. The derived values of the gradient for the thin and the thick discs are in very good agreement with the Lee et al. (2011b) analysis of SEGUE data (who find -22.6 ± 1.6 km s^{-1} dex^{-1} for the thin disc and 45.8 ± 1.8 km s^{-1} dex^{-1} for the thick disc) and with the Adibekyan et al. (2013) measurements in the solar neighbourhood (-16.8 ± 3.7 km s^{-1} dex^{-1} for the thin disc and 41.9 ± 18.1 km s^{-1} dex^{-1} for the thick disc). Our gradient for the thick disc also agrees with the measurements of Kordopatis et al. (2011, 45 ± 12 km s^{-1} dex^{-1}) and Spagna et al. (2010), derived, respectively, from low-resolution FLAMES spectroscopy and SDSS spectro-photometry, with no estimations of [α/Fe]. It also confirms the disagreement with the SDSS result of Ivezić et al. (2008), based on photometric metallicities.

Second, to analyse whether the $\Delta V_\Phi/\Delta$[M/H] value depends on the considered bins of [α/Fe], we derived the mean value of [α/Fe] for each metallicity bin and divided the thick disc sample in two regimes:

- a high-α sample with those bins corresponding to [α/Fe] values higher than the mean [α/Fe] for a given metallicity, and
- a low-α sample with the bins corresponding to lower [α/Fe] values than the mean.

The mean values of [α/Fe] along the thick disc sequence dividing the above defined sub-samples at each metallicity bin are 0.35 dex at [M/H] = −1.0 dex, 0.30 dex at [M/H] = −0.85 dex, 0.25 dex at [M/H] = −0.65 dex, 0.20 dex at [M/H] = −0.45 dex, and 0.15 dex at [M/H] = −0.25 dex. The corresponding derived $\Delta V_\Phi/\Delta$[M/H] slopes are overplotted in Fig. 17. The gradient of rotation with metallicity seems to be steeper than the

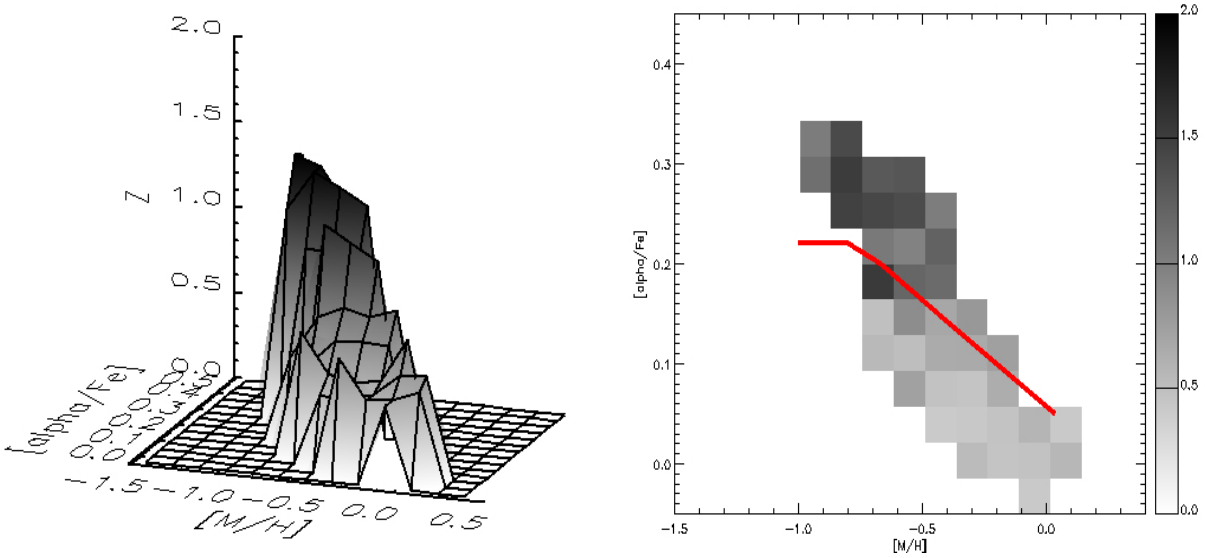

Fig. 15. *Left panel*: 3D plot of the distance to the Galactic plane, in the z-axis, shown as a function of [M/H] and [α/Fe] for the analysed stars (sub-sample *e* of Fig. 12). *Right panel*: distribution of the distances to the Galactic plane in [α/Fe] vs. [M/H]. The red line shows the separation between the thick and the thin disc sequences defined in Sect. 4. In this panel, high-Z values are coded in darker grey than lower Z values.

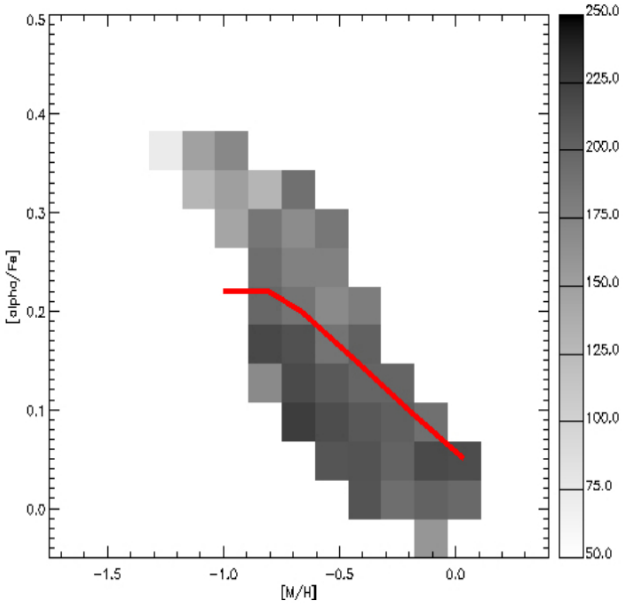

Fig. 16. Distribution of the cylindrical rotational velocity, V_Φ, in the [α/Fe] vs. [M/H] plane. High velocity values are coded in darker grey than lower ones. As in Fig. 15, the red line shows the separation between the thick and the thin discs.

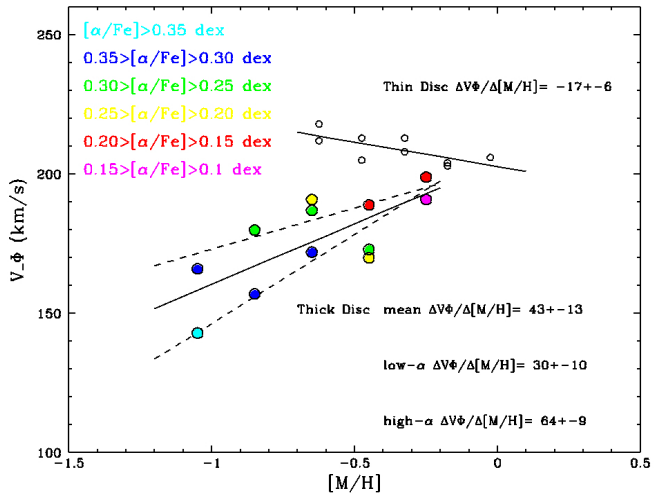

Fig. 17. Rotational velocity gradients with metallicity for the thin (open circles) and thick (filled circles) sequences. The thick disc points are colour-coded by [α/Fe] abundance intervals. The Spearman's rank correlation coefficient between V_Φ and [M/H] is 0.73.

mean (64 ± 9 km s^{-1} dex^{-1} instead of 43 ± 13 km s^{-1} dex^{-1}) when the high-α bins are considered. In contrast, the value of $\Delta V_\Phi/\Delta$ [M/H] is lower than the mean one when it is determined from the low-α bins (30 ± 10 km s^{-1} dex^{-1}). Given that the [α/Fe] dispersion is fairly comparable to the measurement errors, the existence of a real intrinsic dispersion cannot be concluded. Indeed, the described dependence of the $\Delta V_\Phi/\Delta$[M/H] gradient with the considered [α/Fe] bins could be the sign of a contamination of the thick disc stars from the thin disc ones in the lower part of the thick disc sequence. If this is correct, the steeper gradients derived from the high-α bins could be more characteristic of the thick disc population than the previously published ones of about 43 ± 13 km s^{-1} dex^{-1}. To test this possibility, we also derived the value of the slope, using all the bins along the thick disc sequence with a mean error in [α/Fe] lower than 0.04 dex. The resulting slope is 56 ± 19 km s^{-1} dex^{-1} instead of 43 ± 13 km s^{-1} dex^{-1}, confirming that the slope seems steeper for higher quality data.

Finally, to analyse the direct influence of [α/Fe] in the stellar rotation for thick disc stars, we have also derived the correlation between rotation and [α/Fe] separate from [M/H]. As shown in Fig. 18, V_Φ and [α/Fe] are highly anticorrelated (the Spearman's coefficient value is –0.85, corresponding to 0.72% of the V_Φ variance). In addition, the correlation rank between V_Φ and [α/Fe] is even more significant than the one between V_Φ and [M/H] (having a Spearman's coefficient value of 0.73, which accounts for 0.53% of the V_Φ variance).

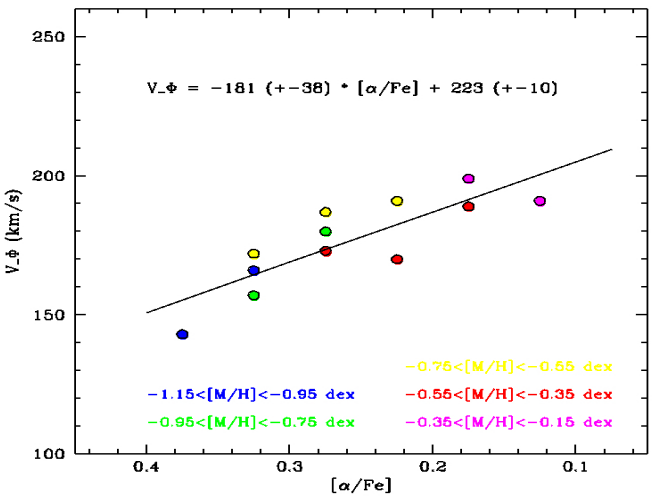

Fig. 18. V_Φ as a function of [α/Fe]for the thick disc sequence stars. The points correspond to the same bins in [α/Fe] and [M/H] than those of Fig. 17 and they are colour-coded by metallicity. The Spearman's rank correlation coefficient between V_Φ and [α/Fe] is –0.85.

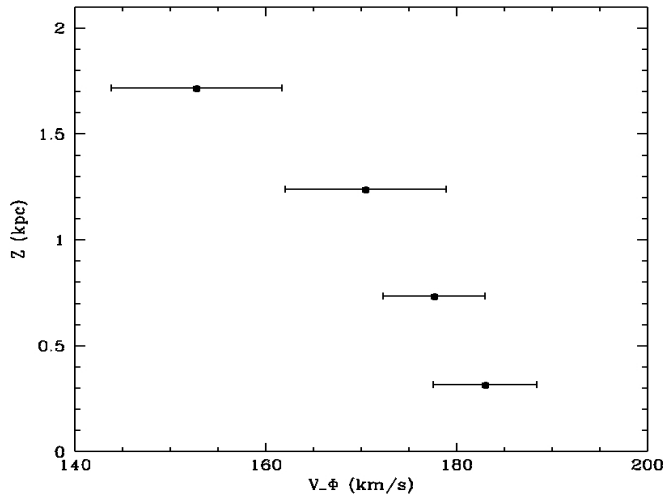

Fig. 19. Mean V_Φ value as a function of vertical height for the thick disc sequence stars.

Furthermore, we checked how azimuthal velocity varies with vertical height for the thick disc sequence stars. Figure 19 shows the mean V_Φ value as a function of Z in four bins of 0.5 kpc. The error bars indicate the standard error of the mean in each bin. Clearly, the azimuthal velocity seems to decrease with height, in particular for Z values higher than about 1 kpc. As a consequence, this could explain why in situ samples of the thick disc can show a higher value of the thick disc lag (hence lower V_Φ values) than the local surveys (see for instance Wyse et al. 2006).

7. Distribution of azimuthal and vertical velocity dispersions

The stellar velocity dispersions can also be studied for the two chemically separated thin and thick disc sequences with our data. To this purpose, since low-quality velocity determinations increase artificially the velocity dispersions, we have further restricted our analysis sub-sample, allowing only stars with errors in azimuthal and vertical velocity lower than 70 km s^{-1}. This value was found to impose a good balance between the statistical robustness and the allowed maximum error in velocity. This new restriction, in addition to those of sub-sample e presented in Table 3, leaves a data set of 645 stars with a mean error in V_Φ of 31 km s^{-1}.

Figure 20 shows the distribution of the measured (not error free) azimuthal and vertical velocity dispersions (σ_Φ and σ_Z) as a function of metallicity and distance to the Galactic plane. The error bars come from the standard error of the derived standard deviations. As expected, both velocity dispersions are higher for the thick disc sequence than for the thin disc one. The mean value of σ_Φ is 54 ± 5 km s^{-1} for the thick disc and 40 ± 3 km s^{-1} for the thin disc. The mean values of σ_Z are 48 ± 5 km s^{-1} for the thick disc sequence and 32 ± 3 km s^{-1} for the thin disc one. As shown in the upper panels of Fig. 20, no significant dependencies of either σ_Φ or σ_Z with metallicity or Z seem to be present in the data. Nevertheless, for the thick disc, the measurements suggest a possible increase in σ_Φ with distance to the Galactic plane that is not visible for σ_Z. This conclusion seems strengthened by the increase in the uncertainty on the derived mean V_Φ values as Z increases, as shown in Fig. 19. A possible decrease of σ_Φ with increasing metallicity could also be present for the thick disc. In addition, around [M/H] ~ -0.3 dex, the dispersion in the azimuthal velocity of the thick and the thin discs seem roughly the same, with a further decrease in σ_Φ for the metal-rich end of the thin disc. This seems to agree with the behaviour of the azimuthal velocity as a function of the metallicity, shown in Fig. 17 (see also Sect. 6). Moreover, the metal-poor side of the thin disc sequence, which presents higher rotation values, also shows a slightly lower azimuthal velocity dispersion.

On the other hand, we point out that our determinations of the velocity dispersions could be affected by the lack of stars at very low Z values (only 37% of the thin disc stars and 17% of the thick disc ones, including the first considered bin of vertical distance, are at abs(z) $<$ 250 pc). This could explain the slightly higher values of dispersion found close to the Galactic plane with respect to other surveys like RAVE (e.g. Burnett 2010).

Finally, for the thick disc sequence, the azimuthal velocity dispersion seems to be similar to the vertical velocity dispersion within the error bars. In any case, the analysed data do not suggest a smaller σ_Φ than the corresponding σ_Z for the thick disc, as predicted by Binney (2012).

8. Orbital parameters

To calculate the orbital parameters of the stars in the sample we integrated orbits in a Galactic potential consisting of a Miyamoto & Nagai (1975) disc, a Hernquist (1990) bulge and a spherical logarithmic halo. Their characteristic parameters took the values $M_{\rm disk} = 9.3 \times 10^{10}\ M_\odot$ and $a = 6.5$ kpc, $b = 0.26$ kpc for the disc, $M_{\rm bulge} = 3 \times 10^{10}\ M_\odot$ and $c = 0.7$ kpc for the bulge, and $v_{\rm h} = 134.5$ km s^{-1}, and $d = 12$ kpc for the halo. In particular, the eccentricities of the stars were defined as $(r_{\rm apo} - r_{\rm peri})/(r_{\rm apo} + r_{\rm peri})$, where $r_{\rm apo}$ ($r_{\rm peri}$) is the maximum (minimum) distance reached by the star in its orbit in the past 2 Gyr.

8.1. Eccentricity distribution

It is widely accepted today that the shape of the eccentricity distribution of the stellar orbits can provide strong constraints on the formation mechanisms of the Galactic disc (Sales et al. 2009). Figure 21 shows the distribution of orbital eccentricities

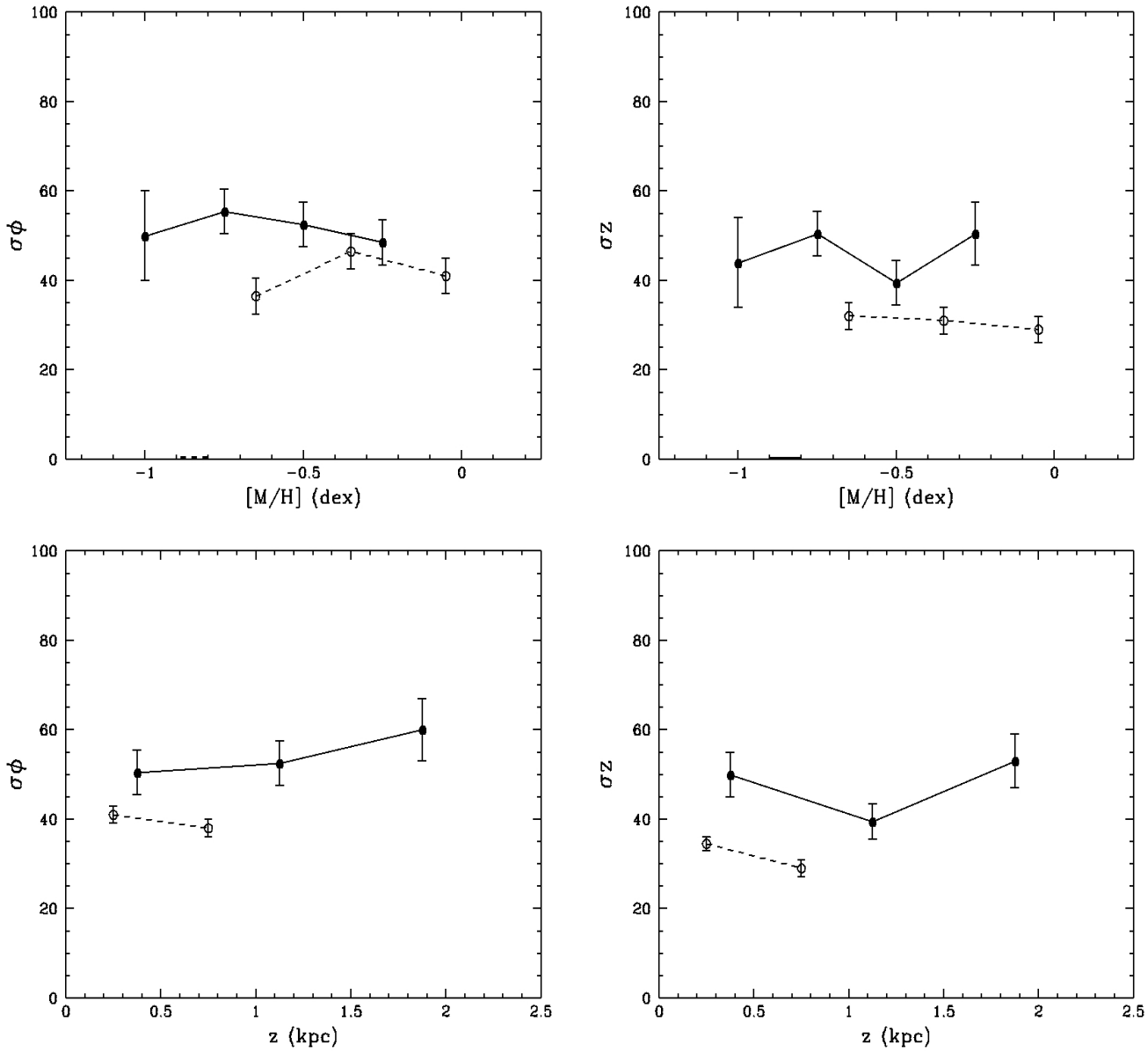

Fig. 20. σ_Φ (*left panels*) and σ_Z (*right panels*) as a function of metallicity (*upper panels*) and distance to the Galactic plane (*lower panels*). Filled circles correspond to the chemically selected thick disc sequence and open circles to the thin disc sequence.

for the thin (red line) and the thick disc (blue line) chemically selected stars. As expected, the thin disc distribution is strongly peaked at a low eccentricity value of ~0.15. On the other hand, the thick disc is significantly broader, and its median eccentricity is around 0.3. Compared to previous determinations, such as those of Wilson et al. (2011), Lee et al. (2011b), and Kordopatis et al. (2011), the shape is flatter and does not decline as fast at high eccentricities, although because of the small number of stars, the significance of this may be questionable.

To evaluate the errors in the computed eccentricities, we calculated the median and the 25% and 75% percentile values of the eccentricity from all orbits starting from 100 realisations of the stars position and velocity and convolved with the errors. Assuming a Gaussian distribution, we derived a value of the standard deviation for each stellar eccentricity. The mean value of the standard deviation depends slightly on the eccentricity itself, and it is equal to 0.14 at eccentricity = 0.20 and 0.13 at eccentricity = 0.80.

Furthermore, Fig. 22 presents the stellar orbital eccentricities as a function of metallicity for the thin and the thick disc sequences (lower and upper panels, respectively). On one hand, the thin disc sequence presents a very similar eccentricity distribution through its whole metallicity range with a majority of low eccentric orbits. In addition, when only thin disc stars with a distance to the plane lower than 400 pc are considered (Fig. 22), most of the thin disc stars with higher eccentric orbits disappear. In addition, this high eccentricity tail of the thin disc suffers from very low statistics and from the relatively large errors in the derived eccentricities. On the other hand, the thick disc sequence seems to present highly eccentric orbits mainly in the metal-poor regime ([M/H] < -0.6 dex). Additionally, the metal-rich part of the thick disc sequence shows very similar eccentricities to the thin disc one. A similar behaviour of the mean eccentricity distribution with metallicity has also been observed by Adibekyan et al. (2013) in the solar neighbourhood. Finally, the derived slopes of the eccentricity dependence on

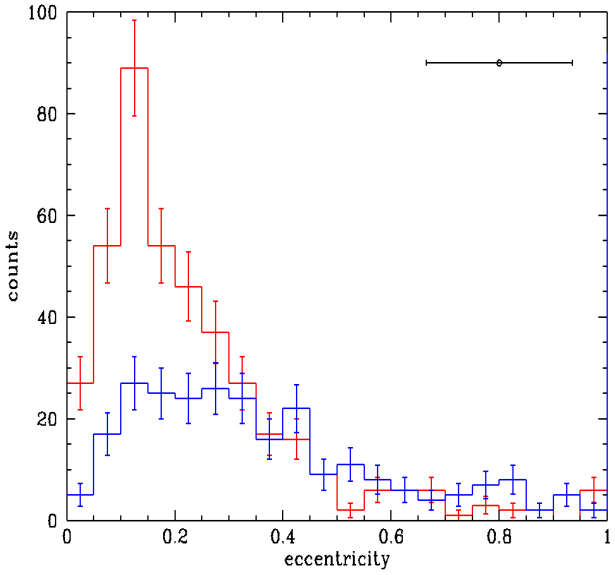

Fig. 21. Eccentricity distributions, with the Poisson uncertainties, for the thin (red) and thick disc (blue) sequences. The typical error bar for the eccentricities is shown in the top right corner of the figure.

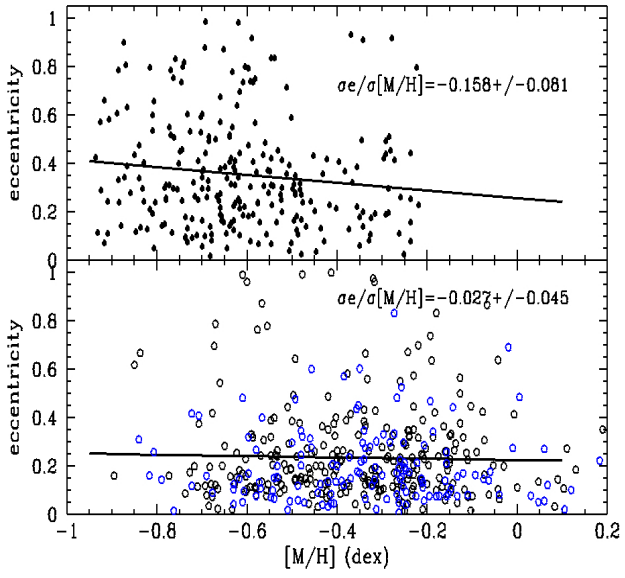

Fig. 22. Stellar orbital eccentricities as a function of metallicity for the thick (*upper panel*) and the thin (*lower panel*) discs. In the *lower panel*, the thin disc stars with distances to the Galactic plane lower than 400 pc are plotted as blue open circles.

metallicity, $\Delta e/\Delta$[M/H], are -0.158 ± 0.081 dex^{-1} for the thick disc and -0.027 ± 0.045 dex^{-1} for the thin disc. These values also agree with those determined by Adibekyan et al. (2013) for the solar neighbourhood (-0.184 ± 0.078 dex^{-1} and -0.023 ± 0.015 dex^{-1} for the thick and the thin disc, respectively).

8.2. Maximum height above the plane

We have also studied the distribution of maximum heights above the Galactic plane, Zmax, for the stars in the thick disc sequence. To this purpose, as shown in Fig. 23, we have plotted the normalized Zmax distribution for three different metallicity intervals.

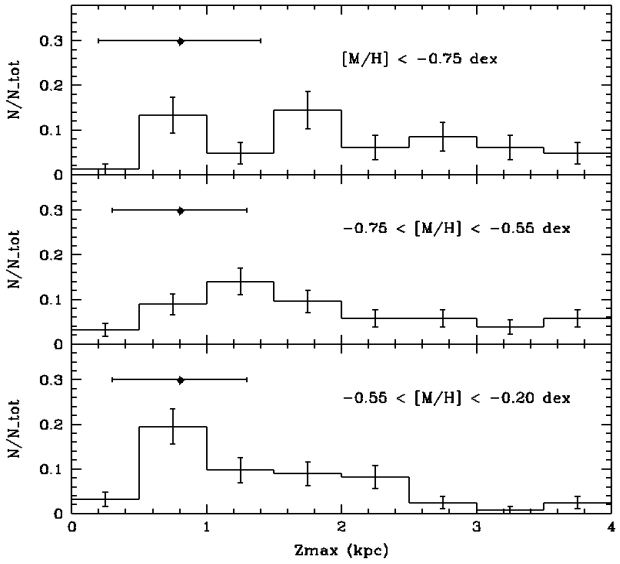

Fig. 23. Normalized distribution of maximum heights above the Galactic plane (Zmax) for the stars in the thick disc sequence, divided into three metallicity intervals. The error bars for the Zmax are shown in the upper left corner of each panel. The Poisson uncertainties are also shown as the histogram's error bars.

The associated error to Zmax was calculated through the procedure described above, which has already been used for the eccentricity error, and it is of the order of 0.6 kpc.

As expected from the analysis of the mean distances to the Galactic plane in Sect. 5, the Zmax distribution seems to peak at lower values as the metallicity increases. Since we are working with a colour/magnitude selected sample, the quantification of a gradient would need correction for the volume sampled as a function of metallicity. Nevertheless, the observed Z and Zmax distributions seem to suggest a rather steep vertical metallicity gradient in the thick disc. On the other hand, Katz et al. (2011) find a low gradient of -0.068 ± 0.009 dex kpc^{-1}, derived without a chemical selection of the thick disc in the [α/Fe] vs. [M/H] plane. On the other hand, Bilir et al. (2012) derived a value of the vertical metallicity gradient in the thick disc of -0.034 ± 0.003 dex kpc^{-1} from a kinematically selected sample of RAVE stars. Finally, Ruchti et al. (2011) find an iron abundance vertical gradient of -0.09 ± 0.05 dex kpc^{-1} for metal-poor thick disc stars.

9. Radial gradients in rotation, metallicity, and [α/Fe]

9.1. The thin disc rotational velocity behaviour with Galactocentric radius

First of all, as illustrated in Fig. 24, we examined a possible dependence of V_Φ on the Galactocentric radius for the thin disc. To this purpose, we selected from the thin disc stars of sub-sample *e* those within a distance to the Galactic plane lower than 700 pc. We also selected stars having errors in V_Φ smaller than 40 km s^{-1} for $7 < R < 9$ kpc up to 60 km s^{-1} for $6 < R < 7$ kpc and $9 < R < 10$ kpc and 50% elsewhere. In addition, we performed a 2-σ clipping around the mean values of V_Φ in three metallicity intervals ([M/H] < -0.5 dex, $-0.5 <$ [M/H] < -0.3 dex, and [M/H] > -0.3 dex). The final sample contains 283 stars

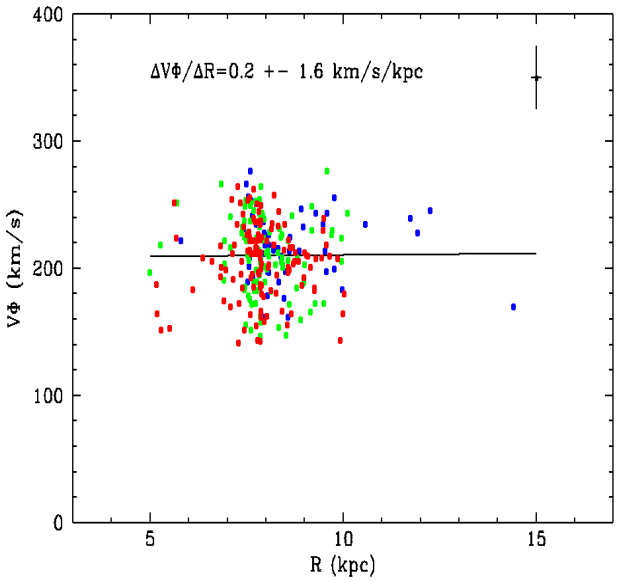

Fig. 24. Rotational velocity gradients with Galactocentric radius for thin disc stars having $|z| < 700$ kpc. The colour codes correspond to three metallicity intervals: [M/H] < -0.5 dex (blue), $-0.5 <$ [M/H] < -0.3 dex (green), and [M/H] > -0.3 dex (red).

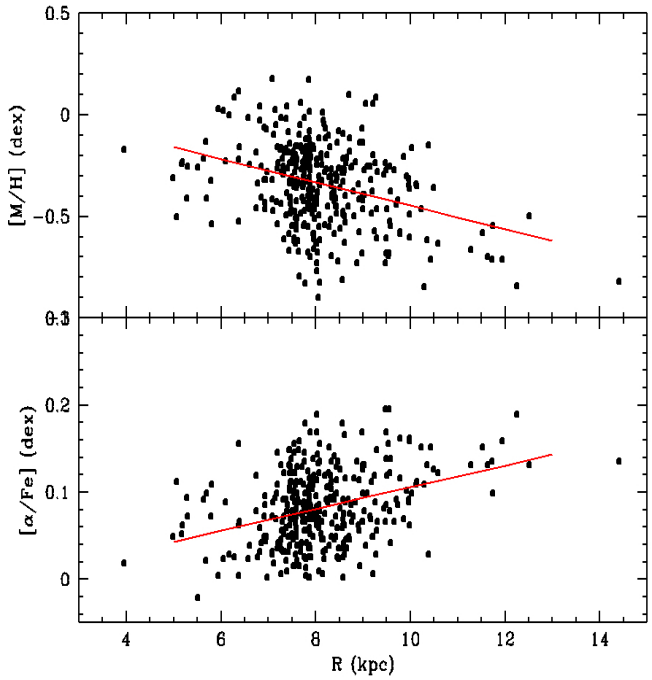

Fig. 25. Global metallicity (*upper panel*) and [α/Fe] (*lower panel*) as a function of the Galactocentric radius for thin disc stars within 700 pc from the Galactic plane.

with a mean error in V_Φ of 23 km s^{-1} and a mean error in R of 130 pc. Owing to the survey selection function for this first GES iDR1 release, most of the thin disc targets near the Galactic plane are within $5 < R < 11$ kpc with very few objects in the outer parts of the disc. The resulting least square fit of the data shows a flat behaviour of the rotational velocity (with a slope of 0.2 ± 1.6 km s^{-1} kpc^{-1}, where the uncertainty comes from the standard error of the slope). For comparison, literature estimations of the Galactic rotation curve from individual velocities of 70 carbon stars by Demers & Battinelli (2007), from gas clouds using the terminal velocities of the HI and CO lines (Sofue et al. 2009), and from APOGEE data (Bovy et al. 2012a) find an approximately flat behaviour, like what is found for the rotational velocity with our data.

In addition, we tested the possible effect of the V_Φ correlation with metallicity (cf. Sect. 6) on the derived V_Φ vs. R relation. To this purpose, we divided the sample described above in three sub-samples for different metallicity intervals: [M/H] $<$ -0.5 dex, $-0.5 <$ [M/H] < -0.3 dex, and [M/H] > -0.3 dex (see Fig. 24). Then, three values of the slope were derived for each of the subsamples. For all these metallicity intervals, the rotational velocity stays flat within the error bar. Therefore, no measurable influence of the stellar rotation correlation with metallicity seems to exist in the thin disc within the studied galactocentric distance range. In agreement with Fig. 17, the mean value of V_Φ decreases with metallicity in the three considered metallicity intervals. Finally, we checked a possible trend in the V_Φ dispersion with R in the examined sample, finding a flat σ_Φ with R in the range $7 < R < 10$ kpc, for which the number of stars allows a robust enough measurement of the V_Φ dispersion.

9.2. Radial abundance gradients

To derive the radial abundance gradients in the thin disc, we used the sample of stars described in Sect. 7.1 and performed least square fits to the [M/H] vs. R distribution and the [α/Fe] vs. R distribution (cf. Fig. 25). We find a negative gradient of -0.058 ± 0.008 dex kpc^{-1} for [M/H] and a very small positive gradient of 0.012 ± 0.002 dex kpc^{-1} for the [α/Fe]. As in the previous section, the uncertainties come from the standard error of the slope, as derived by the least square linear regression.

The value of the metallicity gradient is a matter of debate, ranging from -0.06 to -0.1 dex kpc^{-1}. Our measured value therefore agrees within the literature intervals, such as the most recent studies using Cepheid stars (around -0.06 dex kpc^{-1}, see Lemasle et al. 2013, and references therein[2]) and dwarfs stars in the Corot mission fields (-0.053 ± 0.011 dex kpc^{-1} Gazzano et al. 2013). Measurements based on HII regions[3] range from -0.046 ± 0.009 dex kpc^{-1} to -0.071 ± 0.010 dex kpc^{-1} in the optical and -0.041 ± 0.009 dex kpc^{-1} to -0.085 ± 0.010 dex kpc^{-1} in the infrared (Rudolph et al. 2006). Our metallicity gradient estimation also agrees with the Cheng et al. (2012) analysis of SEGUE data, who find -0.14 dex kpc^{-1} for 0.15 kpc $< Z < 0.25$, -0.082 dex kpc^{-1} for 0.25 kpc$< Z < 0.50$, and -0.024 dex kpc^{-1} for 0.50 kpc $< Z < 1.0$, by selecting low-α stars in their sample. Finally, observations of open clusters find steeper gradients for the inner regions (~ -0.07 dex kpc^{-1} for $R < 12$ kpc, cf. Andreuzzi et al. 2011; Magrini et al. 2009) than for the whole covered radial range (~ -0.05 dex kpc^{-1}, Andreuzzi et al. 2011; Carrera & Pancino 2011). In addition, it is worth noticing that the different above-mentioned indicators trace the gradient at different times, and the issue of the gradient evolution with time is indeed still open.

On the other hand, the very small positive gradient in the [α/Fe] abundance ratio does not seem to be influenced by the cut in vertical distance to the Galactic plane, since its value does not change if the cut is done at $|z| < 400$ pc instead of 700 pc. This could be the case if a contamination by thick disc stars was affecting the radial gradient measurement. However, the presence of numerous metal-poor thin disc stars with [M/H] < -0.5 dex

[2] Measured with iron abundances.
[3] Measured with oxygen, nitrogen, and sulphur abundances.

in our sample influences the measurement, steepening the gradient, because those stars present high values of [α/Fe] and dominate the outer regions. If real, this slightly positive gradient in [α/Fe] could agree with the measurements of Yong et al. (2005) and Carrera & Pancino (2011) for open clusters, Carney et al. (2005) for field giants, and Yong et al. (2006) for Cepheids, who report an enhancement of [α/Fe] in the outer disc. In particular, the result for the Cepheids of Yong et al. (2006) comes from stars in the metal-poor regime ($-1.0 <$ [M/H] < -0.3 dex). Nevertheless, the individual α-element abundances of Cepheids reported by Luck & Lambert (2011) in the range ~4–15 kpc are compatible with a rather small positive gradient in [Mg/Fe], whereas Lemasle et al. (2013) report a [Si/Fe] gradient close to zero and a very small gradient in [Ca/Fe] of 0.016 dex/kpc (assuming the usually accepted metallicity gradient for Cepheids of –0.06 dex/kpc), close to their measurement errors.

Moreover, we have checked the influence of the data spatial distribution in the derived gradients. For that purpose, it is necessary to test the robustness of the two derived gradients on the inhomogeneity of the survey in the R and Z distribution. As already explained in Sect. 5, our total sample is dominated by stars further away from the Galactic plane in the inner parts of the disc with respect to the typical heights probed in regions outside of the solar radius. However, thanks to the restriction of the thin disc sample to Z values below 700 pc, this correlation between Z and R practically dissapears: the mean distance to the Galactic plane is ~450 pc at $R \sim 6$ kpc and ~300 pc at $R \sim 12$ kpc. This small trend cannot be responsible for the measured gradients in metallicity and [α/Fe], especially after the chemical selection of the stars from the thin disc sequence of the [M/H] vs. [α/Fe] plane. In addition, in the case of the [α/Fe] gradient, the small negative trend of Z with R excludes a higher spurious thick disc contamination in the outer regions with respect to the inner ones, as we would expect if the [α/Fe] gradient was artificially created by a bad thin-thick disc separation in the outer regions. Therefore, as a consequence of the two gradients in [M/H] and [α/Fe], the outer parts of the thin disc surveyed by the present sample of GES data (up to $R \sim 12$ kpc) appear more metal-poor and, possibly, slightly richer in [α/Fe] than the inner regions.

Finally, we also analysed the radial abundance gradients in the thick disc population (cf. Fig. 26), selecting stars in the thick disc sequence of the [α/Fe] vs. [M/H] plane with Z distances higher than 700 pc. The cut in Z limits the contamination by thin disc stars and possible problems with the inhomogeneus sampling in R and Z. The derived slopes, both for [M/H] and [α/Fe] for thick disc stars, are within the corresponding error bars (0.006 ± 0.008 dex and -0.004 ± 0.003 dex, respectively). Therefore, our data suggest a flat distribution with galactocentric radius both for [M/H] and [α/Fe] for thick disc stars. Our result for the [M/H] gradient agrees with the Cheng et al. (2012) flat gradient for their selected high-α stars from SEGUE data.

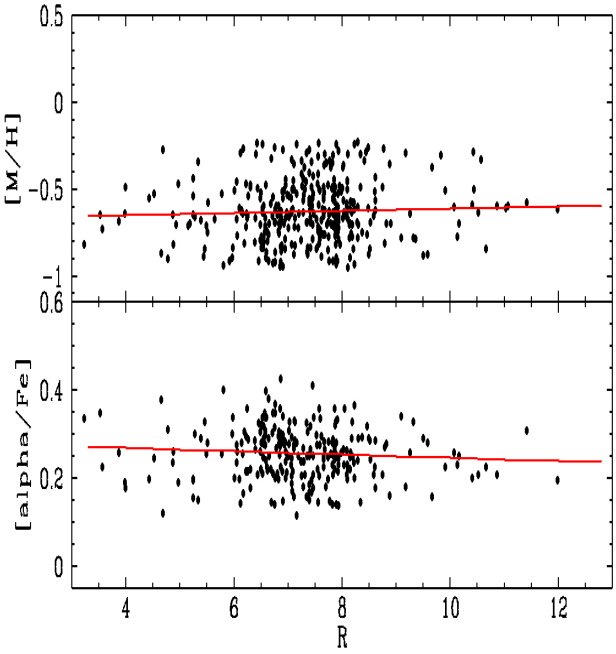

Fig. 26. Global metallicity (*upper panel*) and [α/Fe] (*lower panel*) as a function of the Galactocentric radius for thick disc stars with $Z > 700$ pc from the Galactic plane.

10. Summary and discussion

We used the atmospheric parameters, [α/Fe] abundance ratios, and radial velocities, which were determined from the *Gaia*-ESO Survey GIRAFFE spectra of FGK-type stars (first nine months of observations), to present the kinematical and chemical characterisation of the observed stellar populations. First, we chose to identify the thin to thick disc separation in the [α/Fe] vs. [M/H] plane, thanks to the presence of a low-density region in the number density distribution. This separation agrees with the recently proposed one by Adibekyan et al. (2013) from a sample of solar neighbourhood stars, and the ones observed before by Fuhrmann (2004), Reddy et al. (2006) and Bensby et al. (2007), among others.

Furthermore, we studied the distribution of the distances to the Galactic plane in the [α/Fe] vs. [M/H] plane, with particular attention to the chemically defined thin and thick disc populations. Our results for the thick disc show that the stars lie in progressively thinner layers along the sequence (as metallicity increases and [α/Fe] decreases). This finding could agree with the Haywood et al. (2013) proposal of a thick disc forming stars in thinner and thinner layers for 4–5 Gyr, also predicted by the dissipational settling formation scenario of Burkert et al. (1992). Similarly, Bovy et al. (2012c) have already pointed out the scenario of an evolution in gradually thinner layers (as suggested by the dependence of their scale height distribution on [α/Fe]), although no clear separation between the thin and the thick disc sequences appears in their data. In addition, the recent hydrodynamic simulations of Bird et al. (2013) and Stinson et al. (2013) also show discs in which the younger stars have progressively shorter vertical scale heights. On the other hand, the thin disc sequence presents a constant value of the mean distance to the Galactic plane at all metallicities. As a consequence, the thick to thin disc transition in Z values appears more abrupt in the low-metallicity regime.

Concerning the kinematics, the mean rotational velocities found for the thick and the thin disc sequences are in agreement with the canonical ones ($V_\Phi = 176 \pm 16$ km s^{-1} and $V_\Phi = 208 \pm 6$ km s^{-1}). In addition, the mean Galactic rotation also seems to increase progressively along the thick disc sequence, as the metallicity increases. Our data also confirm the already observed correlations between V_Φ and [M/H] for the two discs. In the case of the thick disc sequence, the mean value of the $\Delta V_\Phi/\Delta$[M/H] is 43 ± 13 km s^{-1} dex^{-1} agrees with the previous findings of Lee et al. (2011b), Kordopatis et al. (2011) and Spagna et al. (2010). This would confirm the disagreement with the SDSS result of Ivezić et al. (2008), based

on photometric metallicities. Moreover, we explored the possible influence of contaminating stars from the thin disc in the analysis of the correlation. If only the stars with the higher [α/Fe] values at each metallicity bin are considered, the derived $\Delta V_\Phi/\Delta$[M/H] is 64 ± 9 km s^{-1} dex^{-1}. As a consequence, this steeper value of the gradient, cleaned from the influence of possible thin disc contaminants could be more characteristic of the real correlation for the thick disc. For the thin disc, a negative gradient of $\Delta V_\Phi/\Delta$[M/H] = −17 ± 6 km s^{-1} dex^{-1} is found. Consequently, the difference in the characteristic rotational velocities between the thin and the thick discs are again accentuated in the low-metallicity regime, as for the mean distances to the Galactic plane. Furthermore, the analysis of the velocity dispersions for the chemically separated thin and thick disc stars confirms a higher dispersion for the thick disc population than for the thin disc one, as expected, for both V_Φ and V_z. Likewise, the stars in the thick and the thin disc sequences also present different distributions of their stellar orbit eccentricities, with the thick disc stars presenting a broader distribution peaked at higher eccentricities than the thin disc one.

Finally, we analysed the properties of the thin and thick discs as a function of the Galactocentric radius. For the thin disc, we estimate a flat behaviour of the thin disc rotational velocity, a metallicity gradient equal to −0.058 ± 0.008 dex kpc^{-1}, and a very small positive [α/Fe] gradient. For the thick disc, no gradients in [M/H] and [α/Fe] are found.

The general picture emerging from our analysis is that of a thick disc that lies in progressively thinner and thinner layers as the metallicity increases and the [α/Fe] decreases with time (until about [M/H] = −0.25 dex and [α/Fe] = 0.1 dex). During this settling process, the thick disc rotation increases progressively and, possibly, the azimuthal velocity dispersion decreases. No measurable metallicity or [α/Fe] gradients with galactocentric distance seem to remain for the thick disc. At about [M/H] = −0.25 dex, the mean characteristics of the thick disc in [α/Fe], vertical distance to the plane, rotation and rotational dispersion are in agreement with (or just slightly different than) that of the thin disc stars of the same metallicity, suggesting a possible connection between the two populations at a certain moment of the disc evolution. This agrees with the Haywood et al. (2013) scenario, in which the inner thin disc (R < 10 kpc) inherited from the chemical conditions left at the end of the thick disc phase (the observed metal-rich end of the thick disc sequence in the [α/Fe] vs. [M/H] plane), some 8 Gyr ago. In their view, there may be an age gap in the star formation that possibly causes the gap in [α/Fe] enrichment, after which star formation proceeds in a thin disc.

For the thin disc, no clear gradient of the mean vertical distance to the plane with the stellar metallicity is observed. On the contrary, the stars in the metal-poor thin disc sequence tail seems to have a mean Galactic rotation velocity higher than those in the metal-rich part. Moreover, if confirmed, the existence of a small positive gradient in [α/Fe] with R leads to a thin disc that would be slightly more metal-poor and [α/Fe]-rich in the outer parts. These two characteristics, similar to those of the metal-poor end of the thin disc sequence in the [α/Fe] vs. [M/H] plane, would favour the picture suggested by Haywood et al. (2013) and Haywood (2006) of this metal-poor thin disc being formed in the outer parts.

Unlike the similarities between the thin and the thick discs around [M/H] ∼ −0.3 dex, the stars in the metal-poor overlapping regime are more clearly separated in their mean physical properties (chemistry, kinematics, possibly orbital eccentricities). This separation seems to be confirmed by the gap (or low-density region) in the [α/Fe] vs. [M/H].

On the other hand, the tight bimodal distribution of [α/Fe] at every value of [M/H] poses severe constraints to model predictions. Recent attempts to define an age-metallicity relation for stars currently in the solar neighbourhood (e.g. Haywood et al. 2013; Mishenina et al. 2013) hint at an evolutionary path in which a very wide range of ages corresponds to a single [M/H] value. The Haywood et al. (2013) results (cf. their Fig. 8) show that at a value of about [M/H] = −0.5 dex stars have an age range around 10 Gyr. On the other hand, the present work and other studies focussed on the solar neighbourhood (e.g. Adibekyan et al. 2013) show that the distribution of [α/Fe] at [M/H] = −0.5 dex appears narrowly bimodal, with two essentially unresolved but quite discrete values of [α/Fe] being found. As a consequence, although stars with [M/H] ≈ −0.5 dex formed over 10 Gyr, they seem to be formed with only two values of [α/Fe]. This is a remarkably severe constraint that can be analysed in light of Galactic models in which radial migration (e.g. Sellwood & Binney 2002; Schönrich & Binney 2009c,b; Roškar et al. 2008) and churning is a major factor.

Schönrich & Binney (2009b) claim that a bimodal, although continuous, distribution of [α/Fe] can naturally come out as a consequence of the standard assumptions about star formation rates and metal enrichment, with no need to invoke breaks in the Galaxy's star formation history or accretion events. However, the tightness of the well populated observed thick and thin disc sequences in the [α/Fe] vs. [M/H] plane, with possibly only two values of [α/Fe] for a given metallicity, poses severe constraints.

If radial migration occurs, one can suppose an evolutionary path in which enrichment in the high-α branch happened rapidly, up to metallicities close to [M/H] = −0.25 dex. This should occur across a wide enough radial range of the proto-Galactic disc. In fact, to preserve the tightness of the high-α sequence, the stars should have formed in a narrow time interval from radially well-mixed interstellar medium (ISM) gas, through all the galactocentric radii that generated stars that are today at a given R (ex. in the solar neighbourhood). Then, to explain the low-α sequence, one can postulate a significant gas accretion, reducing the disc ISM metallicity to, for instance, −0.6 dex. This should be followed by disc evolution in which large scale gas flows (as in fountains, cf. Fraternali et al. 2013, and references therein) retain a tight [α/Fe]-[M/H] correlation, over the radial region which today populates the solar neighbourhood. In addition, this scenario should, somehow, also conciliate the higher rotation values observed in the metal-poor thin disc regime. Otherwise, another possibility for explaining the observed [α/Fe] vs. [M/H] distributions is to suppose that strong radial migration in the sense of churning did not occur (see also the discussion in Haywood et al. 2013).

Finally, this study also shows the importance of precise chemical abundance measurements to solve the stellar population puzzle of the Galactic disc. The stellar chemical patterns can guide the definition of useful stellar sub-samples to unveil the evolutionary paths in the disc formation history and to give clearer constraints to the models. Moreover, in the near future, the *Gaia* mission of the European Space Agency will allow precise distance and age estimations for all the analysed stars. The results presented here, based only on the first months of the GES observations, confirm how crucial large high-resolution surveys outside the solar neighbourhood are today for our understanding of the Milky Way history.

Acknowledgements. Based on data products from observations made with ESO Telescopes at the La Silla Paranal Observatory under programme ID 188.B-3002. The results presented here benefit from discussions held during the *Gaia*-ESO workshops and conferences supported by the ESF (European Science Foundation) through the GREAT Research Network Programme. A. Recio-Blanco, P. de Laverny, and V. Hill acknowledge the support of the French Agence Nationale de la Recherche, under contract ANR-2010-BLAN- 0508-01OTP, and the Programme National de Cosmologie et Galaxies (PNCG) of CNRS/INSU, France. This work was partly supported by the European Union FP7 programme through ERC grant number 320360 and by the Leverhulme Trust through grant RPG-2012-541. We acknowledge the support from INAF and Ministero dell'Istruzione, dell'Università e della Ricerca (MIUR) in the form of the grant Premiale VLT 2012. A. Helmi acknowledges financial support from ERC-Starting Grant, nr. GALACTICA-240271. Finally, we are sincerely grateful to the extremely careful anonymous referee, who without doubt enhanced the value of this paper.

References

Abadi, M. G., Navarro, J. F., Steinmetz, M., & Eke, V. R. 2003, ApJ, 597, 21
Adibekyan, V. Z., Santos, N. C., Sousa, S. G., & Israelian, G. 2011, A&A, 535, L11
Adibekyan, V. Z., Sousa, S. G., Santos, N. C., et al. 2012, A&A, 545, A32
Adibekyan, V. Z., Figueira, P., Santos, N. C., et al. 2013, A&A, 554, A44
Allende Prieto, C., Beers, T. C., Wilhelm, R., et al. 2006, ApJ, 636, 804
Andreuzzi, G., Bragaglia, A., Tosi, M., & Marconi, G. 2011, MNRAS, 412, 1265
Bensby, T. & Feltzing, S. 2010, in IAU Symp. 265, eds. K. Cunha, M. Spite, & B. Barbuy, 300
Bensby, T., Feltzing, S., Lundström, I., & Ilyin, I. 2005, A&A, 433, 185
Bensby, T., Zenn, A. R., Oey, M. S., & Feltzing, S. 2007, ApJ, 663, L13
Bilir, S., Karaali, S., Ak, S., et al. 2012, MNRAS, 421, 3362
Binney, J. 2012, MNRAS, 426, 1328
Bird, J. C., Kazantzidis, S., Weinberg, D. H., et al. 2013, ApJ, 773, 43
Boeche, C., Chiappini, C., Minchev, I., et al. 2013, A&A, 553, A19
Bonifacio, P., Monai, S., & Beers, T. C. 2000, AJ, 120, 2065
Bournaud, F., Elmegreen, B. G., & Martig, M. 2009, ApJ, 707, L1
Bovy, J., Allende Prieto, C., Beers, T. C., et al. 2012a, ApJ, 759, 131
Bovy, J., Rix, H.-W., & Hogg, D. W. 2012b, ApJ, 751, 131
Bovy, J., Rix, H.-W., Liu, C., et al. 2012c, ApJ, 753, 148
Brook, C. B., Kawata, D., Gibson, B. K., & Freeman, K. C. 2004, ApJ, 612, 894
Brook, C., Richard, S., Kawata, D., Martel, H., & Gibson, B. K. 2007, ApJ, 658, 60
Burkert, A., Truran, J. W., & Hensler, G. 1992, ApJ, 391, 651
Burnett, B. 2010, D.Phil Thesis, Oxford University
Carney, B. W., Yong, D., Teixera de Almeida, M. L., & Seitzer, P. 2005, AJ, 130, 1111
Carollo, D., Beers, T. C., Chiba, M., et al. 2010, ApJ, 712, 692
Carpenter, J. M. 2001, AJ, 121, 2851
Carrera, R., & Pancino, E. 2011, A&A, 535, A30
Casetti-Dinescu, D. I., Girard, T. M., Korchagin, V. I., & van Altena, W. F. 2011, ApJ, 728, 7
Cheng, J. Y., Rockosi, C. M., Morrison, H. L., et al. 2012, ApJ, 752, 51
de Laverny, P., Recio-Blanco, A., Worley, C. C., & Plez, B. 2012, A&A, 544, A126
Demarque, P., Woo, J.-H., Kim, Y.-C., & Yi, S. K. 2004, ApJS, 155, 667
Demers, S., & Battinelli, P. 2007, A&A, 473, 143
Edvardsson, B., Andersen, J., Gustafsson, B., et al. 1993, A&A, 275, 101
Fraternali, F., Marasco, A., Marinacci, F., & Binney, J. 2013, ApJ, 764, L21
Freeman, K., & Bland-Hawthorn, J. 2002, ARA&A, 40, 487
Fuhrmann, K. 1998, A&A, 338, 161
Fuhrmann, K. 2004, Astron. Nachr., 325, 3
Fuhrmann, K. 2008, MNRAS, 384, 173
Gazzano, J.-C., Kordopatis, G., Deleuil, M., et al. 2013, A&A, 550, A125
Gilmore, G. & Reid, N. 1983, MNRAS, 202, 1025
Gilmore, G., Randich, S., Asplund, M., et al. 2012, The Messenger, 147, 25
Grevesse, N., Asplund, M., & Sauval, A. J. 2007, Space Sci. Rev., 130, 105
Gustafsson, B., Edvardsson, B., Eriksson, K., et al. 2008, A&A, 486, 951
Harris, W. E. 1996, AJ, 112, 1487
Haywood, M. 2006, MNRAS, 371, 1760
Haywood, M., Di Matteo, P., Lehnert, M., Katz, D., & Gomez, A. 2013, A&A, 560, A109
Hernquist, L. 1990, ApJ, 356, 359
Ishigaki, M. N., Aoki, W., & Chiba, M. 2013, ApJ, 771, 67
Ivezić, Ž., Sesar, B., Jurić, M., et al. 2008, ApJ, 684, 287
Jones, B. J. T., & Wyse, R. F. G. 1983, A&A, 120, 165
Jurić, M., Ivezić, Ž., Brooks, A., et al. 2008, ApJ, 673, 864
Katz, D., Soubiran, C., Cayrel, R., et al. 2011, A&A, 525, A90
Kordopatis, G., Recio-Blanco, A., de Laverny, P., et al. 2011, A&A, 535, A107
Kordopatis, G., Gilmore, G., Wyse, R. F. G., et al. 2013a, MNRAS, 436, 3231
Kordopatis, G., Hill, V., Irwin, M., et al. 2013b, A&A, 555, A12
Lee, Y. S., Beers, T. C., Allende Prieto, C., et al. 2011a, AJ, 141, 90
Lee, Y. S., Beers, T. C., An, D., et al. 2011b, ApJ, 738, 187
Lejeune, T., Cuisinier, F., & Buser, R. 1998, A&AS, 130, 65
Lemasle, B., Francois, P., Genovali, K., et al. 2013, A&A, 558, A31
Liu, C. & van de Ven, G. 2012, MNRAS, 425, 2144
Loebman, S. R., Roškar, R., Debattista, V. P., et al. 2011, ApJ, 737, 8
Luck, R. E., & Lambert, D. L. 2011, AJ, 142, 136
Magrini, L., Sestito, P., Randich, S., & Galli, D. 2009, A&A, 494, 95
McCall, M. L. 2004, AJ, 128, 2144
Minchev, I., & Famaey, B. 2010, ApJ, 722, 112
Minchev, I., Famaey, B., Quillen, A. C., et al. 2012, A&A, 548, A127
Mishenina, T. V., Pignatari, M., Korotin, S. A., et al. 2013, A&A, 552, A128
Misiriotis, A., Xilouris, E. M., Papamastorakis, J., Boumis, P., & Goudis, C. D. 2006, A&A, 459, 113
Miyamoto, M., & Nagai, R. 1975, PASJ, 27, 533
Morrison, H. L., Flynn, C., & Freeman, K. C. 1990, AJ, 100, 1191
Nissen, P. E., & Schuster, W. J. 2010, A&A, 511, L10
Nissen, P. E., & Schuster, W. J. 2011, A&A, 530, A15
Norris, J. E. 1999, Ap&SS, 265, 213
Prochaska, J. X., Naumov, S. O., Carney, B. W., McWilliam, A., & Wolfe, A. M. 2000, AJ, 120, 2513
Quinn, P. J., Hernquist, L., & Fullagar, D. P. 1993, ApJ, 403, 74
Ramírez, I., Allende Prieto, C., & Lambert, D. L. 2013, ApJ, 764, 78
Recio-Blanco, A., Bijaoui, A., & de Laverny, P. 2006, MNRAS, 370, 141
Reddy, B. E., Lambert, D. L., & Allende Prieto, C. 2006, MNRAS, 367, 1329
Reid, M. J. 1993, ARA&A, 31, 345
Rix, H.-W., & Bovy, J. 2013, A&ARv, 21, 61
Roeser, S., Demleitner, M., & Schilbach, E. 2010, AJ, 139, 2440
Roškar, R., Debattista, V. P., Quinn, T. R., Stinson, G. S., & Wadsley, J. 2008, ApJ, 684, L79
Ruchti, G. R., Fulbright, J. P., Wyse, R. F. G., et al. 2011, ApJ, 737, 9
Rudolph, A. L., Fich, M., Bell, G. R., et al. 2006, ApJS, 162, 346
Sales, L. V., Helmi, A., Abadi, M. G., et al. 2009, MNRAS, 400, L61
Schlegel, D. J., Finkbeiner, D. P., & Davis, M. 1998, ApJ, 500, 525
Schlesinger, K. J., Johnson, J. A., Rockosi, C. M., et al. 2012, ApJ, 761, 160
Schönrich, R., & Binney, J. 2009a, MNRAS, 396, 203
Schönrich, R., & Binney, J. 2009b, MNRAS, 396, 203
Schönrich, R., & Binney, J. 2009c, MNRAS, 399, 1145
Schönrich, R., Binney, J., & Dehnen, W. 2010, MNRAS, 403, 1829
Schuster, W. J., Moreno, E., Nissen, P. E., & Pichardo, B. 2012, A&A, 538, A21
Sellwood, J. A., & Binney, J. J. 2002, MNRAS, 336, 785
Smolinski, J. P., Lee, Y. S., Beers, T. C., et al. 2011, AJ, 141, 89
Sofue, Y., Honma, M., & Omodaka, T. 2009, PASJ, 61, 227
Spagna, A., Lattanzi, M. G., Re Fiorentin, P., & Smart, R. L. 2010, A&A, 510, L4
Statler, T. S. 1988, ApJ, 331, 71
Stinson, G. S., Bovy, J., Rix, H.-W., et al. 2013, MNRAS, 436, 625
Valenti, J. A., & Piskunov, N. 1996, A&AS, 118, 595
Villalobos, Á., & Helmi, A. 2008, MNRAS, 391, 1806
Williams, M. E. K., Steinmetz, M., Binney, J., et al. 2013, MNRAS, 436, 101
Wilson, M. L., Helmi, A., Morrison, H. L., et al. 2011, MNRAS, 413, 2235
Wyse, R. F. G., & Gilmore, G. 1995, AJ, 110, 2771
Wyse, R. F. G., Gilmore, G., Norris, J. E., et al. 2006, ApJ, 639, L13
Yong, D., Carney, B. W., & Teixera de Almeida, M. L. 2005, AJ, 130, 597
Yong, D., Carney, B. W., Teixera de Almeida, M. L., & Pohl, B. L. 2006, AJ, 131, 2256
Yoshii, Y. 1982, PASJ, 34, 365
Zwitter, T., Matijevič, G., Breddels, M. A., et al. 2010, A&A, 522, A54

[1] Laboratoire Lagrange (UMR7293), Université de Nice Sophia Antipolis, CNRS, Observatoire de la Côte d'Azur, CS 34229, 06304 Nice Cedex 4, France
e-mail: arecio@oca.eu
[2] Institute of Astronomy, Cambridge University, Madingley Road, Cambridge CB3 0HA, UK
[3] Kapteyn Astronomical Institute, University of Groningen, PO Box 800, 9700 AV Groningen, The Netherlands
[4] Johns Hopkins University, Homewood Campus, 3400 N Charles Street, Baltimore, MD 21218, USA
[5] Centro de Astrofísica da Universidade do Porto, Rua das Estrelas, 4150-762 Porto, Portugal
[6] INAF-Osservatorio Astrofisico di Arcetri, Largo E. Fermi, 5, 50125 Firenze, Italy

[7] Research School of Astronomy and Astrophysics, Australian National University, Canberra, ACT 2611, Australia
[8] Dept. of Astronomy and Theoretical physics, Lund university, Box 43, 22100 Lund, Sweden
[9] Astrophysics Group, Keele University, Keele, Staffordshire ST5 5BG, UK
[10] INAF – Osservatorio Astronomico di Palermo, Piazza del Parlamento 1, 90134 Palermo, Italy
[11] Osservatorio Astronomico di Padova, Vicolo dell-Osservatorio 5, 35122 Padova, Italy
[12] Instituto de Astrofísica de Andalucía (IAA-CSIC), Glorieta de la Astronomía, 18008-Granada, Spain
[13] Instituto de Astrofísica de Canarias, 38205 La Laguna, Tenerife, Spain
[14] INAF-Osservatorio Astronomico di Bologna, via Ranzani 1, Bologna, Italy
[15] Department of Physics and Astronomy, Uppsala University, Box 516, 75120 Uppsala, Sweden
[16] Dipartimento di Fisica e Astronomia, Sezione Astrofisica, Universitá di Catania, via S. Sofia 78, 95123, Catania, Italy
[17] ASI Science Data Center, via del Politecnico SNC, 00133 Roma, Italia
[18] European Southern Observatory, Karl-Schwarzschild-Str. 2, 85748 Garching bei München, Germany
[19] Department for Astrophysics, Nicolaus Copernicus Astronomical Center, ul. Rabiańska 8, 87-100 Toruń, Poland
[20] Moscow M.V. Lomonosov State University, Sternberg Astronomical Institute, Universitetskij pr., 13, 119992 Moscow, Russia